Concentric Conducting Spherical Cavity-Backed Slot Array Applicator

Monai Krairiksh

A Thesis submitted in partial fulfillment of the requirement for the degree

Doctor of Engineering in Electrical Engineering

Graduate School

King Mongkut's Institute of Technology Ladkrabang

1994

ISBN 974-621-141-2

Thesis Title	Concentric Conducting Spherical Cavity-Backed Slot Array Applicator
Student	Mr.Monai Krairiksh
Thesis Advisor	Assoc. Prof.Dr.Wiwat Kiranon
Level of Study	Doctor of Engineering in Electrical Engineering
Department	Telecommunication Engineering, King Mongkut's Institute of Technology Ladkrabang
Year	1994

Abstract

A new type of microwave hyperthermia applicator is proposed and analyzed. A cavity, consists of concentric conducting partial spheres which are enclosed by a part of a conducting cone, is employed to excite an array of slots coherently. From numerical results that be obtained , it shows the feasibility to focus the electric field radiated from the slots to the center of the sphere where a tumor is assumed to be located. SAR distributions of the specific applicators are simulated by computer, and these applicators have been designed for experiment at 2450 MHz. From the measured results of electric field distributions, it is found that the focusing characteristics are available. Thermographic studies show that the heating volume can be varied by using different number of slots and the maximum heating depth at this frequency is 3 cm.

Acknowledgement

It is a great pleasure to express my profound gratitude to Associate Professor Wiwat Kiranon for his valuable guidance, helpful suggestions and encouragement throughout the course of this research.

I am particularly indepted to Professor Toshio Wakabayashi of Tokai University for his significant suggestions and helpful supports.

Professor Kun Mu Chen of Michigan State University and Professor Yoshio Nikawa of The National Defence Academy of Japan contributed notably to the project, without their reference papers this research might be awkward.

I would like to thank Professor Sittichai Pookaiyaudom, President of Mahanakorn University of Technology for his encouragement and support throughout the project. I also wish to thank Assistant Professor Sompol Kosulvit for his hospitality and kindly advicing an additional knowledge during the research.

Valuable discussions and encouragement of Professor Wanlop Surakampontorn and Associate Professor Charay Surawatpunya are sincerely appreciated and acknowledged.

I am deeply grateful to Associate Professor Kobchai Dejhan, Head of Department of Telecommunication Engineering, Mr.Kaname Hiraguri and Mr.Masayasu Komoto, JICA experts, for their kindly supports.

Many parts of the research in this thesis have been carried out with the assistance of a number of persons. Special thanks have been owed to Mr.Kittisak Wayuphak, Mr.Pongphat Noiram, Mr.Montri Thanaphakawat, Mr.Wongsakorn Watcharananunt and Mr.Kittichai Panichpathompong for their great helps. Also, I wish to thank all members of Wakabayashi's Laboratory for their helps.

I wish to thank The National Research Council of Thailand for the financial assistance on the beginning of the project and to the Graduate School for supporting the preparation of this thesis.

Finally, I would like to thank my parents and my family, Mrs.Siraporn, Nawika and Maythus for their understandings, patiences, and loves. Their encouragements provided the necessary motivation to complete the project.

CONTENTS

		page
Chapter 1	Introduction	1
	1.1 Recent Progress of Hyperthermia Cancer Treatment	1
	1.2 Purpose and Scope of the Thesis	2
Chapter 2	Analysis of Interior Electromagnetic Fields from a Slot on a Perfectly Conducting Sphere	4
	2.1 Introduction	4
	2.2 Field Analysis by Vector Spherical Harmonics	5
	2.3 Expansion Coefficients	7
	2.4 Numerical Results	12
	2.5 Conclusion	19
Chapter 3	Electric Field and Specific Absorption Rate from a Spherical Slot Array	20
	3.1 Introduction	20
	3.2 Spherical Slot Array	20
	3.3 Specific Absorption Rate	23
	3.4 Numerical Results	24
	3.5 Conclusion	26
Chapter 4	Concentric Conducting Spherical Cavity	27
	4.1 Introduction	27
	4.2 TM to r Spherical Wave Function	27
	4.3 Concentric Conducting Spherical Cavity	31
	4.4 Numerical Results	33
	4.5 Experimental Results	35
	4.6 Conclusion	37
Chapter 5	Concentric Conducting Spherical Cavity-Backed Slot Array Applicator	38
	5.1 Introduction	38
	5.2 Focus Array	38
	5.3 Concentric Conducting Spherical Cavity-Backed Slot Array Applicator	39
	5.4 SAR Distribution	41
	5.5 Bolus Design	44
	5.6 Conclusion	57
Chapter 6	Performance of the Applicator	58
	6.1 Introduction	58
	6.2 Radiation Patterns	58
	6.3 Input Impedance	64
	6.4 Temperature-Time Relationship	66
	6.5 Heating Patterns	67
	6.6 Conclusion	71

Chapter 7 Discussions and Conclusions 72

References 75

Related Publications 77

Chapter 1

Introduction

1.1 Recent Progress of Hyperthermia Cancer Treatment

Hyperthermia cancer therapy is a treatment procedure in which tumor temperatures are elevated to the range of 43-50°C. The combination of hyperthermia and traditional anticancer treatments is receiving much attention. A recent assessment has indicated that the average complete response with hyperthermia and X-irradition is about 70 percent, compared to only 30 percent with irradiation alone. For a microwave hyperthermia, the method to apply microwave energy into a human body to increase the temperature is divided into two categories; invasive and non-invasive microwave hyperthermia. Invasive hyperthermia has a significant disadvantage that an applicator has to be inserted into the human body which makes the patient harmful. Therefore, non-invasive hyperthermia receives more attention at the expense of difficulty in designing an applicator to fulfill such requirement. A microwave applicator is one that can perform selective heating and plays an important role in a non-invasive hyperthermia cancer treatment [1]. It is employed, without invading into a human body, to apply electric field to elevate temperature of the tumor to a hyperthermic range whereas maintaining the surrounding healthy tissue undamaged. A field penetration depth into the body is inversely proportional to the operating frequency. Using low frequency makes the applicator beamwidth wide at the expense of ineveitably large size. To perform selective heating with a small hotspot size, applicators may be formed in array. The size of an applicator becomes smaller when the operating frequency is higher.

Several types of non-invasive applicator have been investigated in literatures [2-8]. All of them correspond to a kind of a single applicator which are light in weight, simple structure and compact. However they possess a disadvantage that they have no focusing ability, then significant areas of healthy tissue adjacent to the tumor are often heated. The articles in [9-11] introduce that the absorbed power distribution pattern can be modified by arranging the

applicators in array. The use of an array of two microstrip applicators of which the field dirtribution can be controlled by varying an angle between them had been investigated by James *et.al.* [12]. The structure of the array is unfortunately complicated because it needs an external power divider and phase shifter. Lens type applicators have been developed by Nikawa *et.al.*[13-15]. These types of applicators including the one developed by Guy *et .al.* [16] are suitable for a part of the human body that has a cylindrical shape. For some parts of human body such as breast and head which are closely spherical in shape, the author and colleagues [17-19] have proposed an applicator with a rather proper shape and some results have been reported.

1.2 Purpose and Scope of the Thesis

The purpose of this thesis is to research about a microwave hyperthermia applicator made of spherical slot array. A cavity, consists of concentric conducting partial spheres which are enclosed by a part of a conducting cone is employed to excite an array of slots coherently. Calculations are carried out at a frequency of 2450 MHz to investigate the appropriate applicator size for focusing electric field deepen into a human muscle. The medium of interest is limited to the homogeneous human muscle. In the proposed applicator structure, the power divider and the phase shifter are integrated together.

The details in the research can be divided into several chapters as follow:

Chapter 2 deals with the analysis of interior electromagnetic fields from a slot on a perfectly conducting sphere. It describes how to analyze electromagnetic fields radiated from a slot on a perfectly conducting sphere by using vector spherical harmonics. Investigations are performed theoretically to find the electric field distributions in the vicinity of the center of the sphere in terms of slot position, slot length and spherical radius.

Chapter 3 is concerned with the investigation of electric field and specific absorption rate from a slot array on a conducting sphere. Since the configuration of the array is somewhat different from the one described in Chapter 2, by placing array of slots on a part of a

conducting sphere, some modifications on a kind of wave functions must be made. Numerical results associated with electric field from arrays of different number of slots are discussed.

Chapter 4 describes a TM to r spherical wave functions and a concentric conducting spherical cavity. Investigations on the characteristics of such a cavity are performed numerically and are confirmed experimentally. This cavity is employed to excite an array of slots as an applicator.

Chapter 5 presents a concentric conducting spherical cavity backed-slot array applicator. Slots are cut on an inner spherical surface of a concentric conducting spherical cavity and distributions of specific absorption rate from two-slot arrays excited by different cavity modes are illustrated. It is realized that an applicator made of a TM_{02} cavity is suitable for focusing electric field deepen into the heating material. A specific water bolus is proposed and analyzed by solving a heat transfer equation numerically to find the appropriate conditions to eliminate undesirable hotspots.

Chapter 6 presents the experimental results that illustrate the performance of the proposed applicator such as radiation patterns, input impedance, time-relationship and heating patterns. These performance, tested at 2450 MHz, show that the proposed applicator has the capability to focus electric field deepen into a human muscle. The maximum heating depth is 3 cm, which the depth is increased by a factor of 1.8 over that obtained from conventional waveguide applicator. From these investigations, it is realized that this applicator could be used in clinical application as a microwave hyperthermia applicator.

Chapter 7 gives the overall discussions and conclusions of the results obtained from this study and states the recommendation for the further study.

Chapter 2

Analysis of Interior Electromagnetic Fields from a Slot on a Perfectly Conducting Sphere

2.1 Introduction

Since the applicator proposed in this undertaking has partial spherical model, it is essential to investigate, at least theoretically, about the behaviour of the electromagnetic field from a narrow slot in the concentric conducting sphere. This chapter deals with the analysis of the interior electromagnetic field from a slot on a perfectly conducting sphere and some related numerical results. Then the field from the slot array will be discussed in the proceeding chapter.

A perfectly conducting sphere of radius "a" is assumed to be centered at the origin of the cenventional spherical coordinate system (r,θ,ϕ) as shown in Fig.2.1.

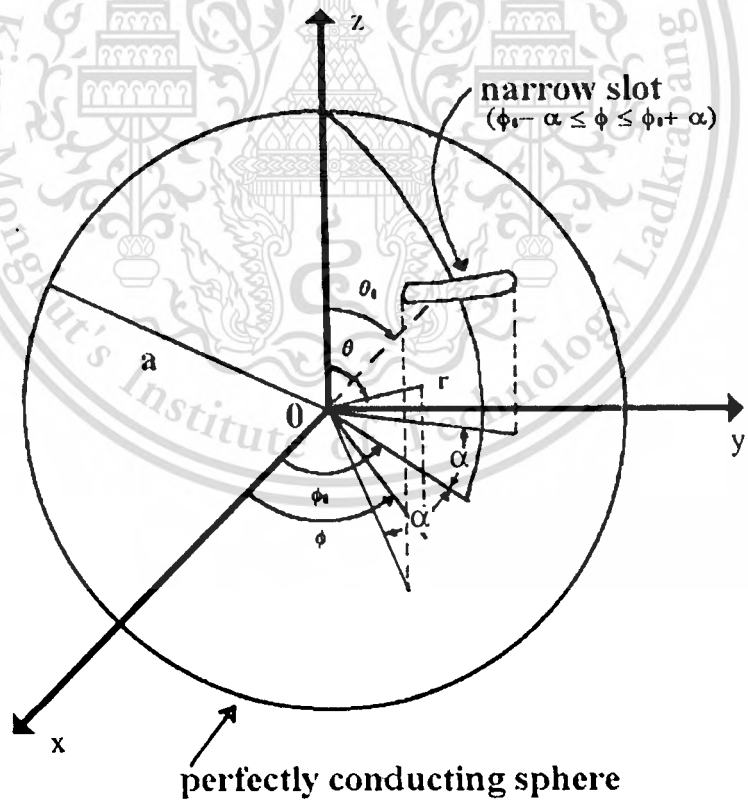

Fig.2.1 Geometry of field calculation from a slot on a conducting sphere

A coordinate (a,θ_0,ϕ_0) locates the center of a narrow slot which its length "l" is specified by an angle 2α. It is horizontally aligned. This slot is assumed to be center excited by an external source. The problem of interest is to evaluate the electromagnetic field in the region inside the sphere.

2.2 Field Analysis by Vector Spherical Harmonics

In this thesis a conventional method for calculating an electromagnetic field is employed because the geometry of the problem is a conducting sphere. This geometry has the general solution in form of the sum of the product of the vector spherical harmonics and the unknown coefficients. These coefficients can be found by matching the boundary condition of the field in the region of interest.

Generally the electric field distribution at the aperture of a slot can be expressed in series of terms of orthogonal set of arbitrary field distribution by a Fourier expansion. However, for a narrow slot at which the field distribution can be recognized as transverses, all field to the slot can be represented in terms of sinusoidal distribution with zero field at the end of the slot. For a realistic conducting sphere, there exists a normal component of the electric field on the spherical surface, imply the existance of induced surface charge [20]. Therefore, the aperture electric field distribution of the slot can be expressed as the followings

$$\mathbf{E}_a(a,\theta,\phi) = \mathbf{a}_r B_{mn}[\mathbf{N}_{mn}(a,\theta,\phi)]$$

$$+ \mathbf{a}_\theta (1/a)\delta(\theta-\theta_o)\cos[\pi(\phi-\phi_o)/2\alpha] \qquad \text{for } \phi_o-\alpha \le \phi \le \phi_o+\alpha$$

$$= 0 \qquad \text{elsewhere} \qquad (2.1)$$

where $\mathbf{a}_r$ and $\mathbf{a}_\theta$ denote unit vectors in r and θ directions, respectively, and δ is the delta function. Also $\mathbf{N}_{mn}$ is a vector spherical harmonics and B_{mn} is a coefficient.

The electromagnetic field maintained by the slot aperture field at any point in space can be expressed in terms of vector spherical harmonics [21,22]. Thus the near-zone electromagnetic field of the slot can be written as

$$\mathbf{E}(r,\theta,\phi) = \sum_{n=0}^{\infty}\sum_{m=-n}^{n}[A_{mn}\mathbf{M}_{mn}(r,\theta,\phi)+B_{mn}\mathbf{N}_{mn}(r,\theta,\phi)] \tag{2.2}$$

$$\mathbf{H}(r,\theta,\phi) = (j/\eta_0)\sum_{n=0}^{\infty}\sum_{m=-n}^{n}[B_{mn}\mathbf{M}_{mn}(r,\theta,\phi)+A_{mn}\mathbf{N}_{mn}(r,\theta,\phi)] \tag{2.3}$$

where the vector spherical harmonics $\mathbf{M}_{mn}$ and $\mathbf{N}_{mn}$ are given as

$$\mathbf{M}_{mn}(r,\theta,\phi)=\mathbf{a}_\theta[\,j_n(kr)(jm/\sin\theta)P^m_n(\cos\theta)e^{jm\phi}\,] - \mathbf{a}_\phi\{j_n(kr)[P^m_n(\cos\theta)]'e^{jm\phi}\} \tag{2.4}$$

and

$$\mathbf{N}_{mn}(r,\theta,\phi)=\mathbf{a}_r\{(1/kr)j_n(kr)n(n+1)P^m_n(\cos\theta)e^{jm\phi}\} + \mathbf{a}_\theta\{(1/kr)[rj_n(kr)]'[P^m_n(\cos\theta)]'e^{jm\phi}\} + \mathbf{a}_\phi\{(1/kr)[rj_n(kr)]'(jm/\sin\theta)P^m_n(\cos\theta)e^{jm\phi}\} \tag{2.5}$$

In (2.4) and (2.5), $j_n(kr)$ represents the first kind of spherical Bessel function of order n. The selection of $j_n(kr)$ is based on the nature of the field that origin of the coordinate system is included. In this analysis $j_n(kr)$ implies an incoming standing wave. The propagation constant k appearing in the expressions of $\mathbf{M}_{mn}$ and $\mathbf{N}_{mn}$ depends on the medium, for the fields in space

$k_0=\omega\sqrt{\mu_0\varepsilon_0}$ and for the fields in the dielectric $k_d=\omega\sqrt{\mu_0\varepsilon}\sqrt{1-j\sigma/\omega\varepsilon}$. $P^m_n(\cos\theta)$ is the associated Legendre function of order n and degree m. η_0 is the impedance of free space and is equal to $\sqrt{\mu_0/\varepsilon_0}$. The coefficients A_{mn} and B_{mn} associated with $\mathbf{M}_{mn}$ and $\mathbf{N}_{mn}$ in (2.2) and (2.3) are to be determined by matching the field on the surface of the conducting sphere.

2.3 Expansion Coefficients

The expansion coefficients A_{mn} and B_{mn} have clearly been derived by Chen et.al.[23] as follows.

If the electric field $\mathbf{E}(a,\theta,\phi)$ given in (2.2) is matched to the slot aperture field $\mathbf{E}_a(a,\theta,\phi)$ in (2.1) on the surface of the conducting sphere at r=a, the following equation is obtained.

$$\sum_{n=0}^{\infty}\sum_{m=-n}^{n}[A_{mn}\mathbf{M}_{mn}(a,\theta,\phi)+B_{mn}\mathbf{N}_{mn}(a,\theta,\phi)]$$

$$= \mathbf{a}_r B_{mn}[\mathbf{N}_{mn}(a,\theta,\phi)]$$

$$+\mathbf{a}_\theta (1/a)\delta(\theta-\theta_0)\cos[\pi(\phi-\phi_0)/2\alpha] \quad \text{for } \phi_0-\alpha\le\phi\le\phi_0+\alpha$$

$$= 0 \qquad \text{elsewhere} \qquad (2.6)$$

The coefficients A_{mn} and B_{mn} can then be determined using orthogonal properties of vector spherical harmonics to be

$$A_{mn} = \frac{\int_0^{2\pi}\int_0^{\pi} \mathbf{a}_\theta(1/a)\delta(\theta-\theta_0)f(\phi).\mathbf{M}_{mn}^*(a,\theta,\phi)\sin\theta d\theta d\phi}{\int_0^{2\pi}\int_0^{\pi} \mathbf{M}_{mn}(a,\theta,\phi).\mathbf{M}_{mn}^*(a,\theta,\phi)\sin\theta d\theta d\phi} \qquad (2.7)$$

$$B_{mn} = \frac{\int_0^{2\pi}\int_0^{\pi} a_\theta (1/a)\delta(\theta-\theta_0) f(\phi).\mathbf{N}_{mn}^{*}(a,\theta,\phi)\sin\theta d\theta d\phi}{\int_0^{2\pi}\int_0^{\pi} \mathbf{N}_{mn}(a,\theta,\phi).\mathbf{N}_{mn}^{*}(a,\theta,\phi)\sin\theta d\theta d\phi} \qquad (2.8)$$

where

$$f(\phi) = \cos[\pi(\phi-\phi_0)/2\alpha] \quad \text{for} \quad \phi_0-\alpha \le \phi \le \phi_0+\alpha$$
$$= 0 \quad \text{elsewhere} \qquad (2.9)$$

From (2.4) and (2.5) we see that $\mathbf{M}_{mn}$ and $\mathbf{N}_{mn}$ can be divided into two parts

$$\mathbf{M}_{mn}(r,\theta,\phi) = \mathbf{M}_{emn}(r,\theta,\phi) + j\,\mathbf{M}_{omn}(r,\theta,\phi) \qquad (2.10)$$

$$\mathbf{N}_{mn}(r,\theta,\phi) = \mathbf{N}_{emn}(r,\theta,\phi) + j\,\mathbf{N}_{omn}(r,\theta,\phi) \qquad (2.11)$$

where

$$\begin{Bmatrix} \mathbf{M}_{emn}(r,\theta,\phi) \\ \mathbf{M}_{omn}(r,\theta,\phi) \end{Bmatrix} = \mp a_\theta \,(m/\sin\theta)\, j_n(kr)\, P^m{}_n(\cos\theta) \begin{Bmatrix} \sin m\phi \\ \cos m\phi \end{Bmatrix}$$
$$-a_\phi\, j_n(kr)\, \frac{d\,P^m{}_n(\cos\theta)}{d\theta} \begin{Bmatrix} \cos m\phi \\ \sin m\phi \end{Bmatrix} \qquad (2.12)$$

$$\begin{Bmatrix} N_{emn}(r,\theta,\phi) \\ N_{omn}(r,\theta,\phi) \end{Bmatrix} = a_r \left\{ \frac{n(n+1)j_n(kr)P^m{}_n(\cos\theta)}{kr} \begin{Bmatrix} \cos m\phi \\ \sin m\phi \end{Bmatrix} \right\}$$

$$+a_\theta \left\{ (1/kr) \frac{d[rj_n(kr)]}{dr} \frac{dP^m{}_n(\cos\theta)}{d\theta} \begin{Bmatrix} \cos m\phi \\ \sin m\phi \end{Bmatrix} \right\}$$

$$\mp a_\phi \left\{ (1/kr) \frac{d[rj_n(kr)]}{dr} jm \frac{P^m{}_n(\cos\theta)}{\sin\theta} \begin{Bmatrix} \sin m\phi \\ \cos m\phi \end{Bmatrix} \right\} \quad (2.13)$$

Therefore,

$$M^*{}_{mn}(a,\theta,\phi) = M_{emn}(a,\theta,\phi) - j\, M_{omn}(a,\theta,\phi) \quad (2.14)$$

$$N^*{}_{mn}(a,\theta,\phi) = N_{emn}(a,\theta,\phi) - j\, N_{omn}(a,\theta,\phi) \quad (2.15)$$

$$\int_0^{2\pi}\int_0^{\pi} M_{mn}(a,\theta,\phi).\, M_{mn}{}^*(a,\theta,\phi)\, \sin\phi d\theta d\phi$$

$$= \int_0^{2\pi}\int_0^{\pi} [\, |M_{emn}(a,\theta,\phi)|^2 + |M_{omn}(a,\theta,\phi)|^2] \sin\theta d\theta d\phi \quad (2.16)$$

$$\int_0^{2\pi}\int_0^{\pi} N_{mn}(a,\theta,\phi).N_{mn}{}^*(a,\theta,\phi)\, \sin\theta d\theta d\phi$$

$$= \int_0^{2\pi}\int_0^{\pi} |N_{emn}(a,\theta,\phi)|^2 + |N_{omn}(a,\theta,\phi)|^2] \sin\theta d\theta d\phi \quad (2.17)$$

According to Ref.[23],

$$\int_0^{2\pi}\int_0^{\pi} \mathbf{M}_{emn}(a,\theta,\phi)^{2} \sin\theta d\theta d\phi = \frac{(1+\delta_m)\, 2\pi\, (n+m)!}{(2n+1)(n-m)!}\, n(n+1)\, [j_n(k_0a)]^2 \qquad (2.18)$$

$$\int_0^{2\pi}\int_0^{\pi} \mathbf{N}_{emn}(a,\theta,\phi)^{2} \sin\theta d\theta d\phi = \frac{(1+\delta_m)\, 2\pi}{(2n+1)^2}\, \frac{(n+m)!}{(n-m)!}\, n(n+1)$$

$$.\{(n+1)[j_{n-1}(k_0a)]^2\} + n[j_{n+1}(k_0a)]^2\} \qquad (2.19)$$

where $\delta_m=1$ if $m=0$ and $\delta_m=0$ if $m>0$.

On the other hand, since $f(\phi)$ and the θ-component of $\mathbf{M}_{omn}(a,\theta,\phi)_\theta$ and $\mathbf{N}_{emn}(a,\theta,\phi)_r$, $(\mathbf{M}_{emn})_\phi$ and $(\mathbf{N}_{emn})_\theta$, are even functions of variable ϕ while $(\mathbf{M}_{emn})_\theta$ and $(\mathbf{N}_{omn})_\theta$ are odd functions of ϕ, the numerators of (2.7) and (2.8) can be evaluated as follows.

$$\int_0^{2\pi}\int_0^{\pi} \mathbf{a}_\theta(1/a)\delta(\theta-\theta_0)f(\phi).\mathbf{M}_{mn}^{*}(a,\theta,\phi)\sin\theta d\theta d\phi$$

$$=-j\int_0^{2\pi}\int_0^{\pi} (1/a)\delta(\theta-\theta_0)f(\phi)\,[\mathbf{M}_{omn}(a,\theta,\phi)]_\theta \sin\theta d\theta d\phi \qquad (2.20)$$

$$\int_0^{2\pi}\int_0^{\pi} \mathbf{a}_\theta(1/a)\delta(\theta-\theta_0)\, f(\phi).\, \mathbf{N}_{mn}^{*}(a,\theta,\phi)\, \sin\theta d\theta d\phi$$

$$= \int_0^{2\pi}\int_0^{\pi} (1/a)\delta(\theta-\theta_0)\, f(\phi)\, [\mathbf{N}_{emn}(a,\theta,\phi)]_\theta \sin\theta d\theta d\phi \qquad (2.21)$$

Substituting the expressions for $f(\phi)$, $(\mathbf{M}_{omn})_\theta$ and $(\mathbf{N}_{emn})_\theta$ from (2.9), (2.12) and (2.13) into the right hand side of (2.20) and (2.21), we have

$$\int_0^{2\pi}\int_0^{\pi} a_\theta(1/a)\delta(\theta-\theta_0)\, f(\phi).\, \mathbf{M}_{mn}^{*}(a,\theta,\phi)\, \sin\theta d\theta d\phi$$

$$= -j\, j_n(k_0a)\, \frac{m\, P^m{}_n(\cos\theta_0)}{a}.\, \frac{4\pi\alpha\cos m\alpha}{\pi^2-4m^2\alpha^2} \qquad (2.22)$$

$$\int_0^{2\pi}\int_0^{\pi} a_\theta(1/a)\delta(\theta-\theta_0)\, f(\phi).\, \mathbf{N}_{mn}^{*}(a,\theta,\phi)\, \sin\theta d\theta d\phi$$

$$= \frac{[aj_n(k_0a)]'}{k_0a^2}\, [P^m{}_n(\cos\theta_0)]'\, \sin\theta_0\, \frac{4\pi\alpha\cos m\alpha}{\pi^2-4m^2\alpha^2} \qquad (2.23)$$

where $[P^m{}_n(\cos\theta_0)]' = \frac{d[P^m{}_n(\cos\theta)]}{d\theta}\Big\}_{\theta=\theta_0}$

$$[aj_n(k_0a)]' = \frac{d[rj_n(k_0r)]}{dr}\Big\}_{r=a}$$

Substituting (2.16) through (2.19), (2.22) and (2.23) into (2.7) and (2.8), we obtain the experssions for the coefficients A_{mn} and B_{mn} as

$$A_{mn} = \frac{-j\, m\alpha\, \cos m\alpha}{a(\pi^2-4m^2\alpha^2)}\, \frac{(2n+1)}{(1+\delta_m)n(n+1)}\, \frac{(n-m)!}{(n-m)!}\, \frac{P^m{}_n(\cos\theta_0)}{j_n(k_0a)} \qquad (2.24)$$

$$B_{mn} = \frac{\alpha\cos m\alpha\, (2n+1)^2}{\pi^2-4m^2\alpha^2}\, \frac{(n-m)!}{(n+m)!}\, \frac{\sin\theta_0\, [P^m{}_n(\cos\theta_0)]'}{n(n+1)\, k_0a^2(1+\delta_m)}$$

$$\frac{[aj_n(k_0a)]'}{.\, \{(n+1)[j_{n-1}(k_0a)]^2+n[j_{n+1}(k_0a)]^2\}} \qquad (2.25)$$

Once A_{mn} and B_{mn} are obtained, the near-zone field of the slot is completely determined.

2.4 Numerical Results

It is remarkable that there are four important parameters, to the field distributions, in the expressions derived in section 2.3; spherical radius (a), slot position (θ_0,ϕ_0), angle of the slot (α) and slot length (l). It is desirable to find the parameters that makes the field maximum at the center of the sphere. This can be accomplished by mean of computer calculation. For our numerical examples in free space to be discussed, we have calculated electric field at a specific point (center of the sphere) and varied the value of n .It was found to be sufficient to set n=15 because as we increased the number of n more than these values, the result did not change significantly. Fig.2.2 shows the convergent criteria of the calculation.

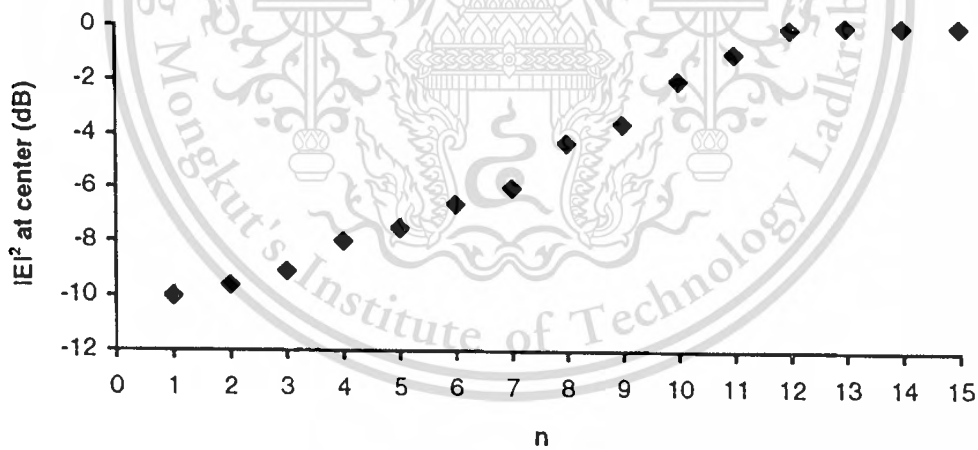

Fig.2.2 Convergent criteria of the calculation

First the frequency was specified at 1,650 MHz, α was fixed at 2.2 rad and the slot was positioned at θ_0=0.58 rad and ϕ_0=0 rad. Power, which is proportional to square of electric field at the center of the sphere, was calculated. By varying the spherical radius in calculations, it is

found that the maximum value of the electric field takes place when the radius a is equal to 4.4 cm. Keeping the spherical radius at this value and the angle α is changed with the slot position at the same position, the field is maximum when α is 2.31 rad. After that keeping α and the spherical radius a and then varying θ_0, it is found that the maximum of the field occurs when θ_0 is 0.59 rad, for α equals to 2.31 rad and a is 4.4 cm. This process was repeated until the maximum value does not significantly change, the parameters that provide the maximum of the field at the center of the sphere become a is 4.4 cm, θ_0= 0.59 rad and α is 2.31 rad, respectively.

Calculations were also performed with the same process at the frequency of 434, 915, 2,450 and 3,000 MHz respectively. Variations of these parameters, that provide the maximum of the field at the center of the sphere, for different frequencies are plotted as shown in Fig.2.3. It is noted that the parameters that provide the maximum field at the center of the sphere have different values at different operating frequencies. For an angle of a slot, it is in the range of 0.17 - 0.23 rad. The slot position is in the range of 0.42 - 0.6 rad. The spherical radius and the slot length are inversely proportional to the operating frequency as shown in Fig.2.3.

When the frequency has been adjusted, the frequency response of the slot on sphere that provide maximum field at the center of the sphere are illustrated in Fig.2.4. It is observed that the bandwidth of the slot on a sphere that provides the maximum of the field at the center of the sphere is very narrow. For the case of the operating frequency of 915 MHz, the bandwidth is 0.87%. At the operating frequency of 1.65 GHz, 2.45 GHz and 3.0 GHz the bandwidth is 4.6%, 4.57% and 4.33% respectively.

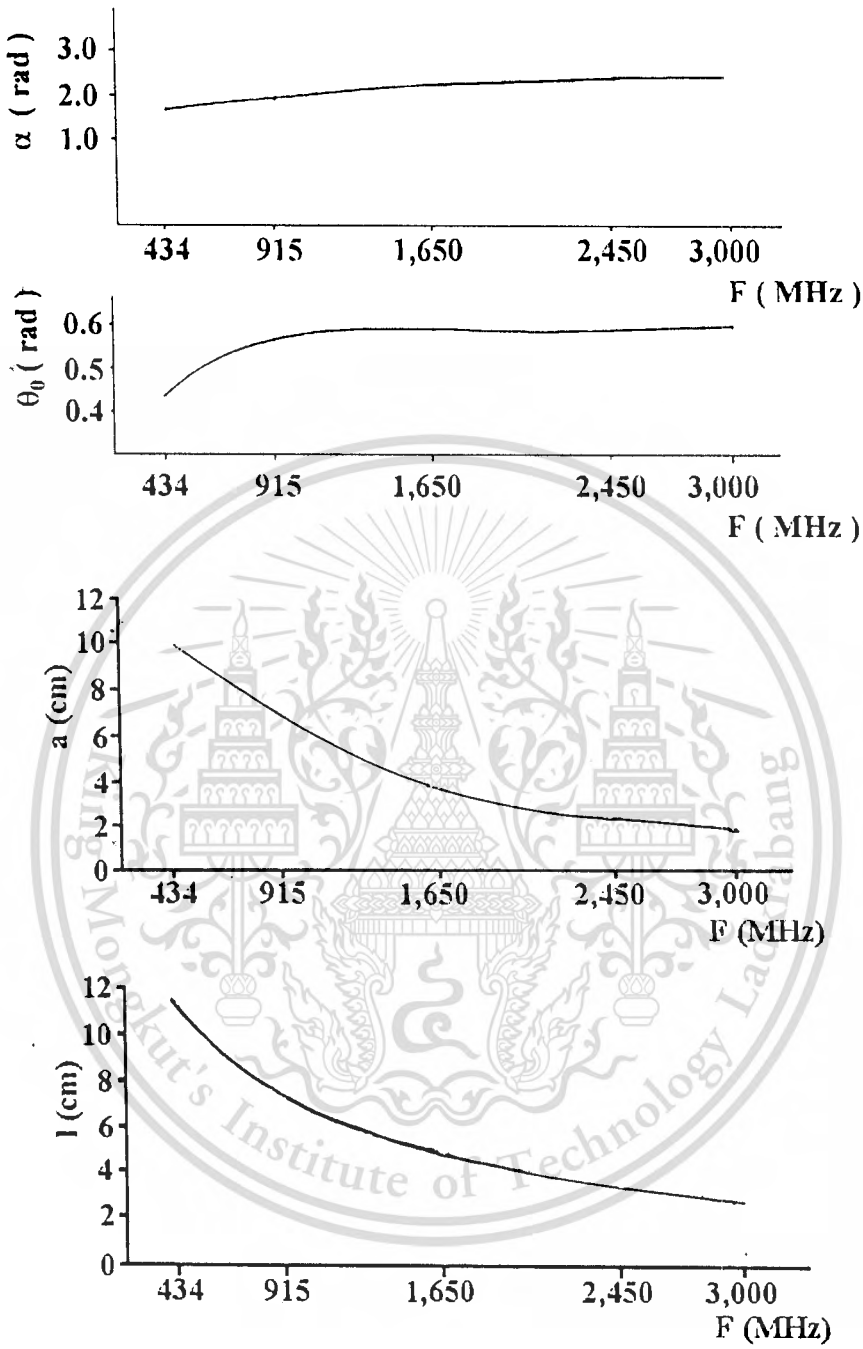

Fig.2.3 Variation of parameters that provide the maximum of the field at the center of the sphere

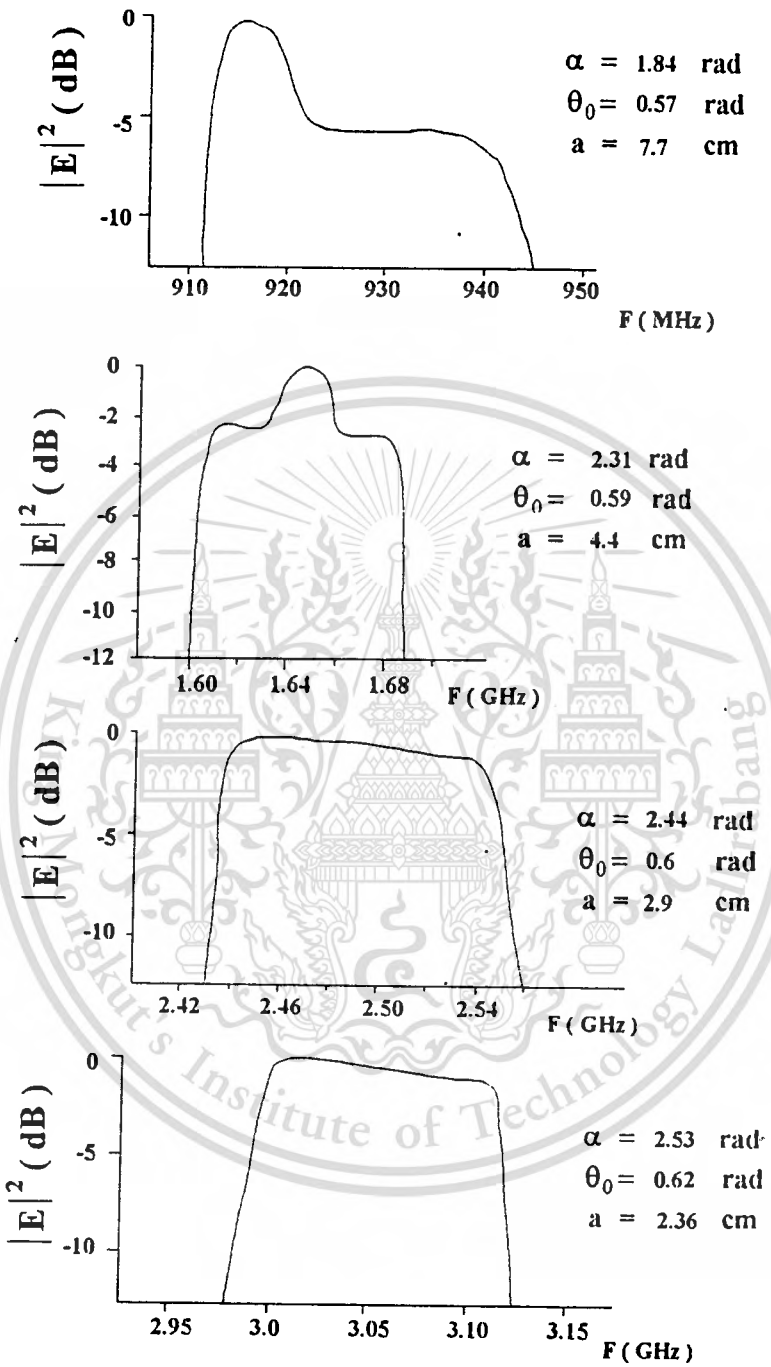

Fig.2.4 Frequency response of slot on sphere that provides maximum field at the center of the sphere

Patterns of electric field from a slot on a sphere, with arbitrary dimensions, were evaluated. Fig.2.5 shows the power pattern, on the z=0 plane in two principal planes, of a slot on a sphere with f= 2,450 MHz, α= 2.0 rad, a= 4.3 cm and θ_0= 0.785 rad. It is found that on this plane, the field appeared maximum at the center of the sphere. The power pattern of this slot, at 1,000 MHz and 3,000 MHz, were carried out and plotted as shown in Fig.2.6 and Fig.2.7, respectively. It is noticable that the maximum of the field still takes place at the center of the sphere.

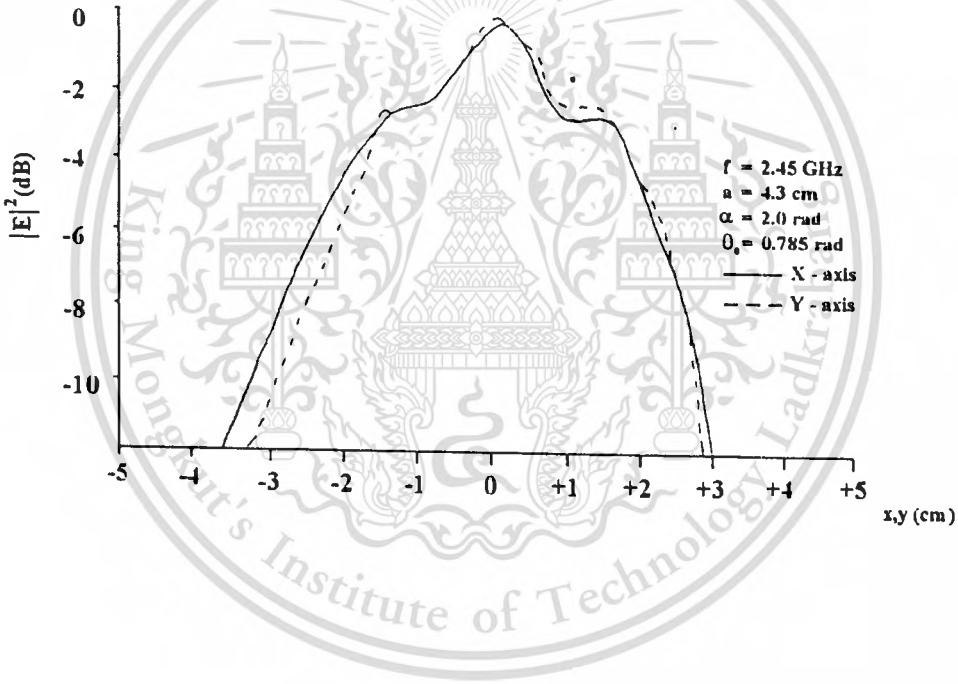

Fig.2.5 Power pattern on the z=0 plane

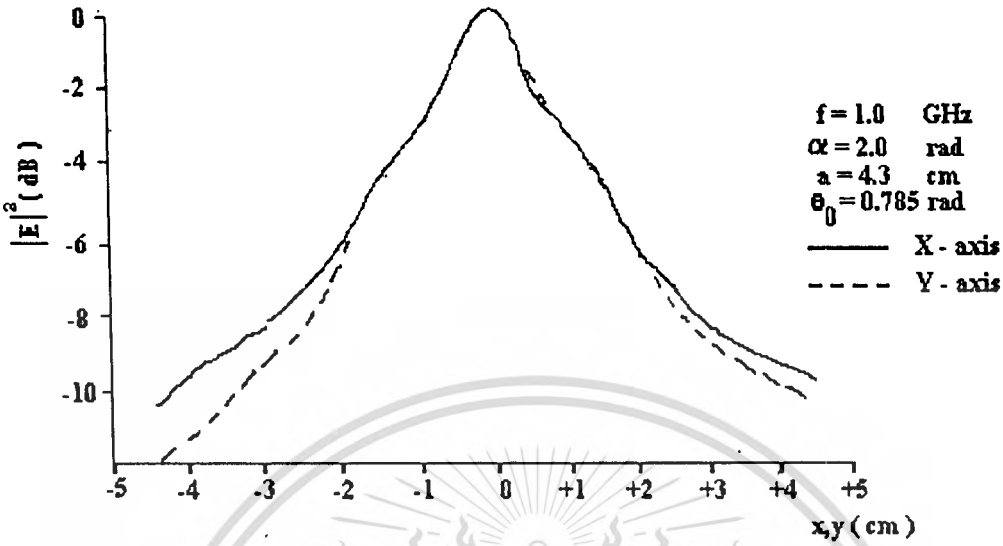

Fig.2.6 Power pattern at 1000 MHz

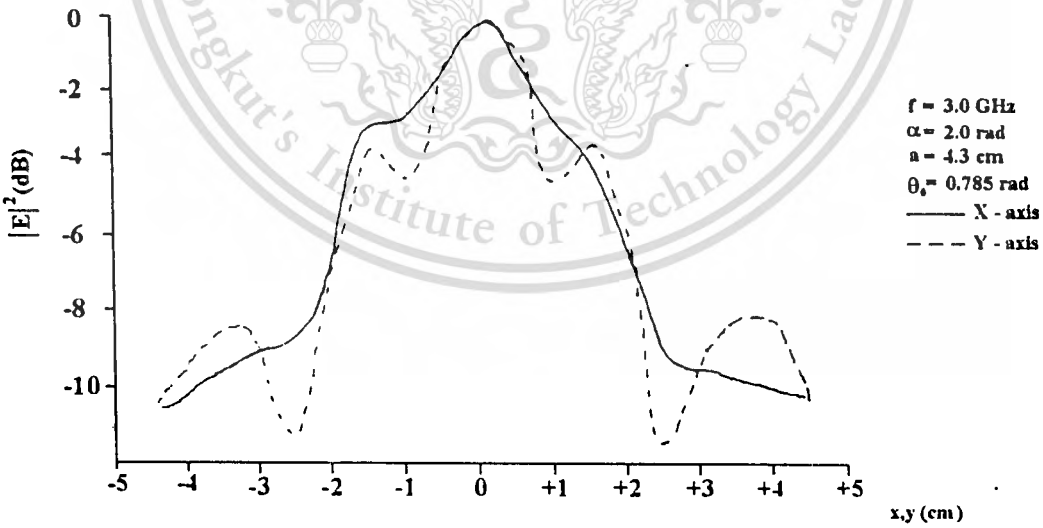

Fig.2.7 Power pattern at 3000 MHz

At the frequency of 2,450 MHz, using α= 2.0 rad, a= 4.3 cm, θ_0= 0.785 rad and ϕ_0= 0 rad, the vàriation of squared-electric field along the z axis is displayed in Fig.2.8. The field is symmetry along the z axis because the structure is a close sphere and a standing wave along this direction is symmetry. The two - dimensional pattern is shown in Fig.2.9. Is it obvious that the maximum of the field occurs at the center of the sphere.

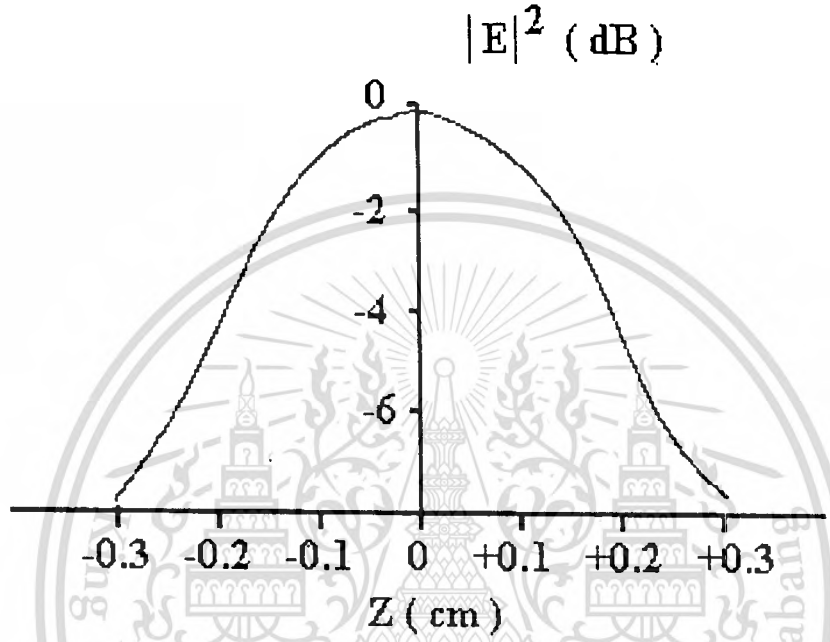

Fig.2.8 Variation of squared- electric field along the z axis

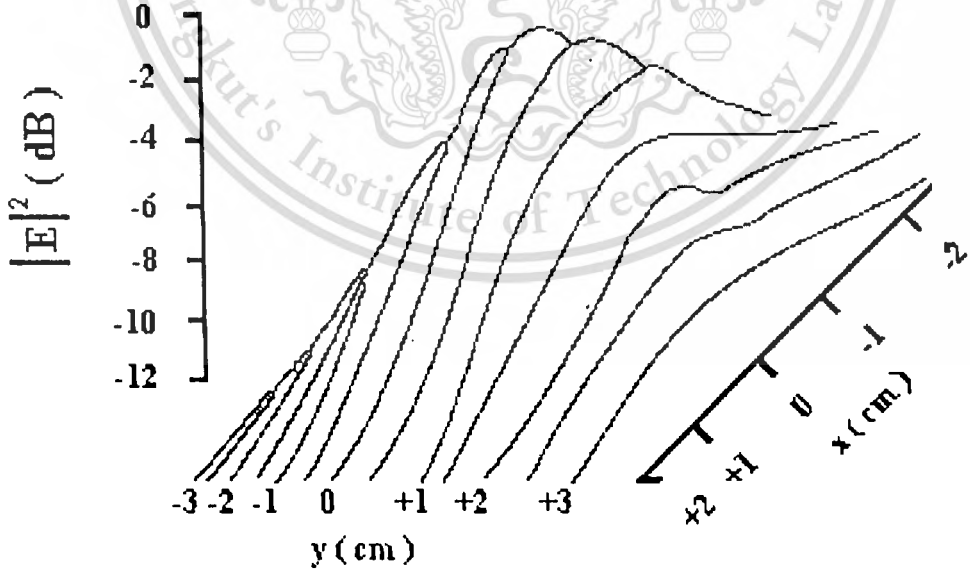

Fig.2.9 Two - dimensional pattern

2.5 Conclusion

In this chapter, the expressions for interior field of a slot on a conducting sphere are derived in terms of vector spherical harmonics. The electric field intensity are evaluated and the parameters that provide the maximum electric field intensity at the center of the sphere are illustrated. Most of investigation in this chapter deals with the structure that is a full sphere, that will form a basic concept for the proposed applicator which possesses the structure of a partial sphere. Therefore, some modifications will be performed and described in Chapter 3.

Chapter 3
Electric Field and Specific Absorption Rate from a Spherical Slot Array

3.1 Introduction

In chapter 2 the behaviours of electromagnetic field from a slot on a perfectly conducting sphere have been revealed. It shows the interesting character of focus ability at the center. For the sake of application, some modifications of structure are considered in this chapter; the slots are assumed to be aligned on a part of a sphere. SAR are also taken into account.

3.2 Spherical Slot Array

Let us assume that there are n slots, each slot is identified by the number i (i=1,2,...,n), located at $(a,\theta_{oi},\phi_{oi})$ on the surface of a part of a spherical conductor of radius "a". The edge of the surface is situated at the conical angle θ_c. Each slot is "l" meter long which subtend angle on the azimuthal plane of it is 2α rad. The geometry of the problem is displayed in Fig.3.1.

Electric field at an arbitrary position (r,θ,ϕ) is calculated by using the vector spherical harmonics as described in chapter 2. The electric field from the *ith* slot is

$$E(r,\theta,\phi) = \sum_{n=0}^{\infty} \sum_{m=-n}^{n} [A_{mn}\mathbf{M}_{mn} + B_{mn}\mathbf{N}_{mn}] \qquad (3.1)$$

where $\mathbf{M}_{mn}$ and $\mathbf{N}_{mn}$ are the vector spherical harmonics.

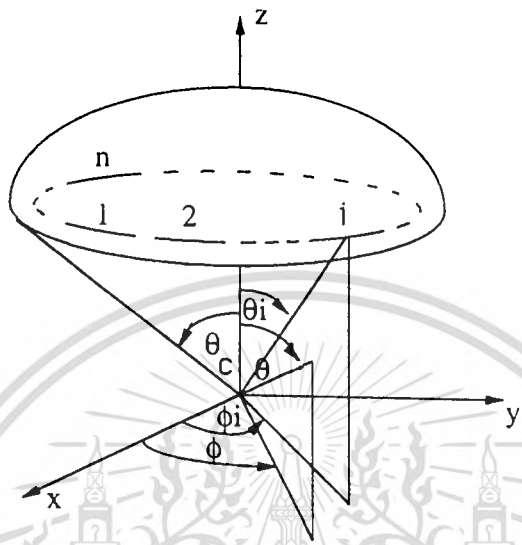

Fig.3.1 Geometry of a spherical slot array

Since the problem considered in this chapter is somewhat modified; the electric field propagates from the slot on a part of a sphere and the medium is assumed to be a homogeneous lossy material, to simulate the human muscle, instead of a lossless one. Therefore, the appropriate vector spherical harmonics in (3.1) will be modified to be

$$M_{mn} = a_\theta \frac{jm\, h_n^{(1)}(kr)\, P^m{}_n\cos(\theta)\, e^{jm\varphi}}{\sin\theta} + a_\varphi\, h_n^{(1)}(kr) \frac{dP^m{}_n\cos(\theta)}{d\theta} e^{jm\varphi} \qquad (3.2)$$

and

$$N_{mn} = \frac{a_r \{n(n+1)\, h_n^{(1)}(kr)\, P^m{}_n(\cos\theta)\, e^{jm\varphi}\}}{kr}$$

$$+a_\theta \left\{ \frac{1}{kr} \frac{d}{dr}[rh_n^{(1)}(kr)] \frac{d\, P^m{}_n(\cos\theta)}{d\theta}\, e^{jm\varphi} \right\}$$

$$-a_\varphi \left\{ \frac{1}{kr} \frac{d}{dr}[rh_n^{(1)}(kr)] \frac{jm\, P^m{}_n(\cos\theta)}{\sin\theta}\, e^{jm\varphi} \right\} \qquad (3.3)$$

In order to determine the values of the expansion coefficients A_{mn} and B_{mn}, the method illustrated in chapter 2 is also utilized. One of the keypoints is to set the boundary condition of the electric field at the slot aperture to match to the radiated field on the aperture. Moreover, the orthogonal properties of the vector spherical harmonics have to be utilized. According to the lossy medium in the space $\theta>\theta_c$, it is presumed that electric field at θ greater than θ_c vanishes and mutual coupling is negligible. Hence, integration of θ from 0 to π will change to from 0 to θ_c and the expansion coefficients can be expressed as

$$A_{mn} = \frac{-jm\alpha P^m{}_n(\cos\theta_o)\cos(m\alpha)\cos(m\phi_o)}{a(\pi^2-4m^2\alpha^2)(1+\delta_m)n(n+1)} \int_0^{\theta c} [P^m{}_n(\cos\theta)]^2 \sin\theta d\theta \qquad (3.4)$$

and

$$B_{mn} = \frac{\pi\alpha\cos(m\alpha)\cos(m\phi_o)}{ka^2(\pi^2-4m^2\alpha^2)n(n+1)} \int_0^{\theta c} [P^m{}_n(\cos\theta_o)]^2 \sin\theta d\theta$$

$$\frac{[P^m{}_n(\cos\theta_o)]' \sin\theta_o [ah^{(1)}{}_n(ka)]'}{[\{(1+\delta_m)\pi/2(2n+1)\}\{(n+1)[h^{(1)}{}_{n-1}(ka)]^2+n[h^{(1)}{}_{n+1}(ka)]^2\}+n(n+1)\alpha[h^{(1)}{}_n(ka)/ka]^2]} \qquad (3.5)$$

where , δ_m =1 if m=0

=0 if m≠0

and

$h^{(1)}_n(.)$: spherical Hankel function of the first kind is chosen to express an inward traveling wave.

$k= \omega \sqrt{(\mu_o \varepsilon)(1-j\sigma/\omega\varepsilon)}$.

The resultant electric field from every slot can be calculated by summing up the the field from each slot. That is

$$E_T = \sum_{i=1}^{n} E_i \qquad (3.6)$$

E_T is the total electric field from the slot array and E_i (i=1,2,...n) is the electric field from the *i th* slot.

3.3 Specific Absorption Rate

An outstanding performance of a focused hyperthermia applicator is its capability that can deposit the energy of electromagnetic field in the form of heat and produce a hotspot.The details about the position and size of the hotspot can be revealed by investigation about electric field distribution and Specific Absorption Rate (SAR). SAR is the quantity that is defined by the derivative of the incremental energy absorbed by an incremental mass contained in a volume element [24]. It is related to the temperature rise of heating material by

$$SAR=4184\, c(dT/dt) \quad (W/kg) \qquad (3.7)$$

where c is the specific heat of the material to be heated (kcal/kg °C), T is temperature (°C) and t is time (second). SAR is also expressed as

$$SAR=(0.5\sigma/\rho)\,|\mathbf{E}_T|^2 \qquad (W/kg) \qquad (3.8)$$

where σ and ρ are the conductivity (S/m) and density (gm/cc) of the medium, respectively and $\mathbf{E}_T$ is the resultant electric field induced in the heating material.

The effective field size (EFS) is the area that the temperature rise is half of the maximum temperature and is defined by a 50 % SAR contour [25].

3.4 Numerical Results

Since SAR is proportional to magnitude square of electric field intensity, the investigation of squared- electric field distribution of slot arrays are performed in this section. They are the field from two-slot, three-slot and four-slot array, respestively. These arrays are cut on a part of a conducting sphere of radius "a" m. The edge of the sphere is at $\theta=54.5^0$ and each slot is located at a conical angle of 45^0. For the two-slot array, each slot is 9.25 cm long. The length of the slots in the three-slot and four-slot arrays are 6.0 and 4.5 cm respestively. Calculations are performed in the human muscle with $\varepsilon_r= 49.6$ and $\sigma=1.0$ S/m at the frequency of 2450 MHz [13].

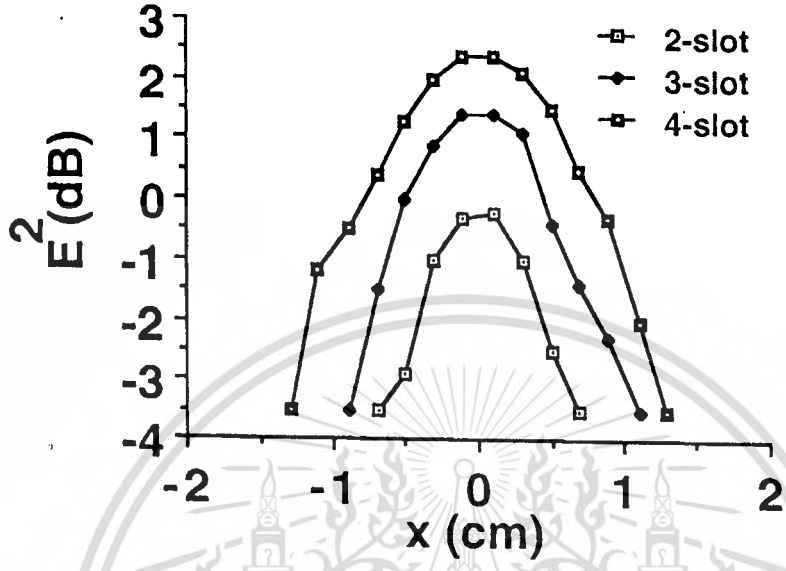

(a) along x-axis

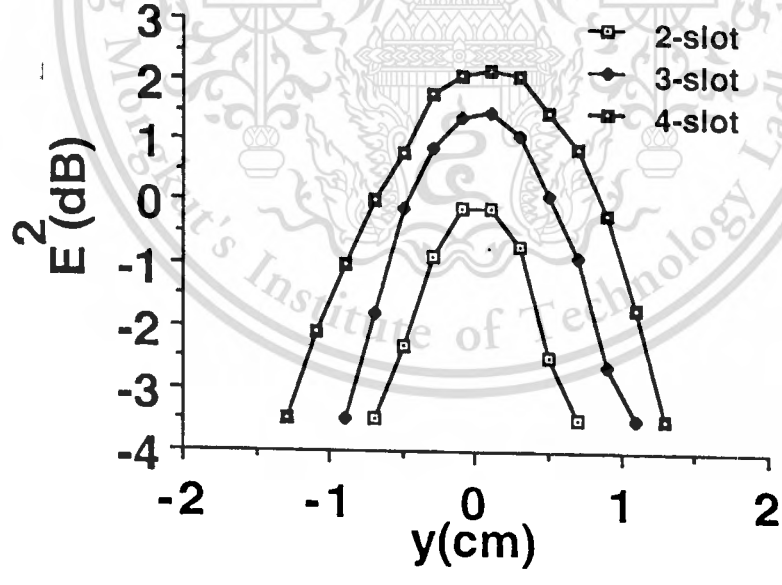

(b) along y-axis

Fig.3.2 Squared- electric field distribution

Fig.3.2 shows the squared - electric field distribution computed on the focal plane of these slot arrays . From the results, we can determine the EFS. It is observed that the -3 dB beamwidth which corresponds to the EFS of the two-slot applicator is 1.1 cm on the x-axis and 1.2 cm on the y-axis. For the three-slot array the EFS is slightly larger than the case of the two-slot, and the peak amplitude is 1.5 dB higher than that of the two-slot one. Moreover for the four-slot array, the -3 dB beamwidth is 1.9 cm in both x and y directions with the peak amplitude of 2.5 dB higher than the two-slot array. This implies that the EFS can be controlled by using different number of slots .

3.5 Conclusion

This chapter concerns with calculation of electric field from a slot array on a part of a spherical conductor. Since the medium of interest is assumed to be a homogeneous lossy material, the field from the slot array is assumed to be a traveling inward wave. Hence, spherical Hankel function of the first kind is employed.

Chapter 4

Concentric Conducting Spherical Cavity

4.1 Introduction

This chapter describes about the cavity used to excite the applicator. Since applicator of interest is spherical in shape, it is reasonable to excite it by spherical cavity. In the undertaking research, the spherical slot array applicator is supposed to be excited by a concentric conducting spherical cavity. By this way the cavity will excite the slots coherently and protects against radiation hazard which may harm the nearby person and the patient oneself. Since this cavity is excited by a coaxial transmission line, therefore, a TM wave to radial direction is generated in this cavity.

4.2 TM to r- Spherical Wave Function

Transverse magnetic (TM) modes are field configurations whose magnetic field components lie in a plane that is transverse to a given direction. That direction is often chosen to be the path of wave propagation [26]. By examining

$$\mathbf{H} = \mathbf{a}_r\left[-j\omega F_r + \frac{1}{\mu r\sin\theta}\left[\frac{\partial}{\partial\theta}(A_\phi\sin\theta) - \frac{\partial A_\theta}{\partial\phi}\right]\right.$$

$$\left.\frac{-j}{\omega\mu\varepsilon}\left\{\frac{\partial}{\partial r}\left[\frac{1}{r^2}\frac{\partial}{\partial r}(r^2F_r)\right] + \frac{1}{r\sin\theta}\frac{\partial}{\partial\theta}(\sin\theta F_\theta) + \frac{1}{r\sin\theta}\frac{\partial F_\phi}{\partial\phi}\right]\right\}\Bigg]$$

$$+ a_\theta \left[-j\omega F_\theta + \frac{1}{\mu r}\left[\frac{1}{\sin\theta}\frac{\partial A_r}{\partial \phi} - \frac{\partial (rA_\phi)}{\partial r}\right]\right.$$

$$\left. \frac{-j}{\omega\mu\varepsilon}\left\{\frac{1}{r}\frac{\partial}{\partial\theta}\left[\frac{1}{r^2}\frac{\partial (r^2F_r)}{\partial r}\right] + \frac{1}{r\sin\theta}\frac{\partial}{\partial\theta}(\sin\theta F_\theta) + \frac{1}{r\sin\theta}\frac{\partial F_\phi}{\partial\phi}\right]\right\}\right]$$

$$+ a_\phi \left[-j\omega F_\phi + \frac{1}{\mu r}\left[\frac{\partial (rA_\theta)}{\partial r} - \frac{\partial A_r}{\partial\theta}\right]\right.$$

$$\left. \frac{-j}{\omega\mu\varepsilon}\left\{\frac{1}{r\sin\theta}\frac{\partial}{\partial\phi}\left[\frac{1}{r^2}\frac{\partial (r^2F_r)}{\partial r}\right] + \frac{1}{r\sin\theta}\frac{\partial}{\partial\theta}(\sin\theta F_\theta) + \frac{1}{r\sin\theta}\frac{\partial F_\phi}{\partial\phi}\right]\right\}\right] \quad (4.1)$$

where A_r, A_θ, A_ϕ and F_r, F_θ, F_ϕ are the component vector of the magnetic vector potential and electric vector potential, respectively.

It is evident from (4.1) that to derive the field expressions that are TM to r (which H_r=0), it is sufficient to let the vector potential A have only a component in such r direction. The another components of A as well as all of F are set equal to zero. Let

$$A = A_r(r,\theta,\phi) \quad (4.2a)$$

$$F = 0 \quad (4.2b)$$

where the ratio A_r/r, and not A_r, is a solution to a scalar Helmholtz wave equation

$$(\nabla^2+\beta^2)A_r/r = 0 \quad (4.3)$$

where β is the phase constant (rad/m).

It should be noted that the A_r component can be excited by placing an electric probe parallel to the electric field lines; Er [26].

The electric and magnetic field components can be written in terms of A_r as follows

$$\mathbf{E_A} = \frac{1}{j\omega\mu\varepsilon} \nabla x \nabla x \mathbf{A} \tag{4.4}$$

or

$$E_r = \frac{1}{j\omega\mu\varepsilon}\left(\frac{\partial^2}{\partial r^2} + \beta^2\right) A_r \tag{4.4a}$$

$$E_\theta = \frac{1}{j\omega\mu\varepsilon} \frac{1}{r} \frac{\partial^2 A_r}{\partial r \partial \theta} \tag{4.4b}$$

$$E_\phi = \frac{1}{j\omega\mu\varepsilon} \frac{1}{r\sin\theta} \frac{\partial^2 A_r}{\partial r \partial \phi} \tag{4.4c}$$

and

$$H_A = \frac{1}{\mu} \nabla x \mathbf{A} \tag{4.5}$$

or

$$H_r = 0 \tag{4.5a}$$

$$H_\theta = \frac{1}{\mu} \frac{1}{r\sin\theta} \frac{\partial A_r}{\partial \phi} \tag{4.5b}$$

$$H_\varphi = \frac{-1}{\mu}\,\frac{1}{r}\,\frac{\partial A_r}{\partial \theta} \qquad (4.5c)$$

A_r/r is a solution to (4.3).

Eq.(4.3) can be expressed in the form

$$(\nabla^2+\beta^2)\psi \qquad (4.6)$$

where

$$\psi = A_r/r \qquad (4.6a)$$

Since the solution of ψ from (4.6) must be multiplied by r to obtain solution for A_r, the appropriate solution for A_r must be equal to the product of $r\psi$. The solution for A_r of (4.6) through (4.6a) can be expressed in the seperable form as

$$A_r(r,\theta,\phi) = f(r)g(\theta)h(\phi) \qquad (4.7)$$

where $f(r)$, $g(\theta)$ and $h(\phi)$ must be represented by appropriate wave functions that satisfy the wave equation in spherical coordinate. According to the solutions of the wave equation in the θ direction are in the form of associated Legendre functions $P^m{}_n(\cos\theta)$ and $P^m{}_n(-\cos\theta)$ for n= interger and $P^m{}_n(\cos\theta)$ and $Q^m{}_n(\cos\theta)$ for n= interger, the Legendre functions become infinite either at $\theta=0$ or $\theta=\pi$ unless n is interger; hence for free space n must be an interger.Therefore the $g(\theta)$ can be represented by associated Legendre functions of the first $P^m{}_n(\cos\theta)$ kind or second $Q^m{}_n(\cos\theta)$ kind whereas $h(\phi)$ can be represented by a sinusoidal function.

Since the solutions of ψ in (4.6) must be multiplied by r in order to obtain solutions to A_r as given by (4.7), it is most convenient to represent f(r) not by spherical Bessel $[j_n(\beta r), y_n(\beta r)]$

functions, but by other form of spherical Bessel functions denoted by $\hat{B}_n(\beta r)$ [for either $\hat{J}_n(\beta r)$ or $\hat{Y}_n(\beta r)$]. These are related to the regular spherical Bessel function denoted by $b_n(\beta r)$ [for either $j_n(\beta r)$ or $y_n(\beta r)$] as

$$\hat{B}_n(\beta r) = \beta r b_n(\beta r) = \beta r\sqrt{\frac{\pi}{2\beta r}}\, B_{n+1/2}(\beta r) = \sqrt{\frac{\pi\beta r}{2}}\, B_{n+1/2}(\beta r) \qquad (4.8)$$

where $B_{n+1/2}(\beta r)$ is used to represent the regular cylindrical Bessel functions of $J_{n+1/2}(\beta r)$ and $Y_{n+1/2}(\beta r)$.

Therefore the solution for f(r) of (4.7) are of the new form of spherical Bessel functions denoted by

$$f(r) = A\hat{J}_n(\beta r)+B\hat{Y}_n(\beta r) \qquad (4.9)$$

4.3 Concentric Conducting Spherical Cavity

A cross-section of the concentric partial spherical cavity is shown in Fig.4.1. It consists of concentric conducting spheres with inner and outer radii "a" and "b", respectively. Assume that their centers are at the origin of the spherical coordinate system, and the edge of the partial spherical conductors are enclosed by a part of a conducting cone at an angular angle of θ_c. The maximum field, corresponds to the maximum of surface current density is assumed to take place at θ_0. When the cavity of this structure is excited by a coaxial transmission line along the z-axis, a transverse magnetic wave will be generated inside the cavity.

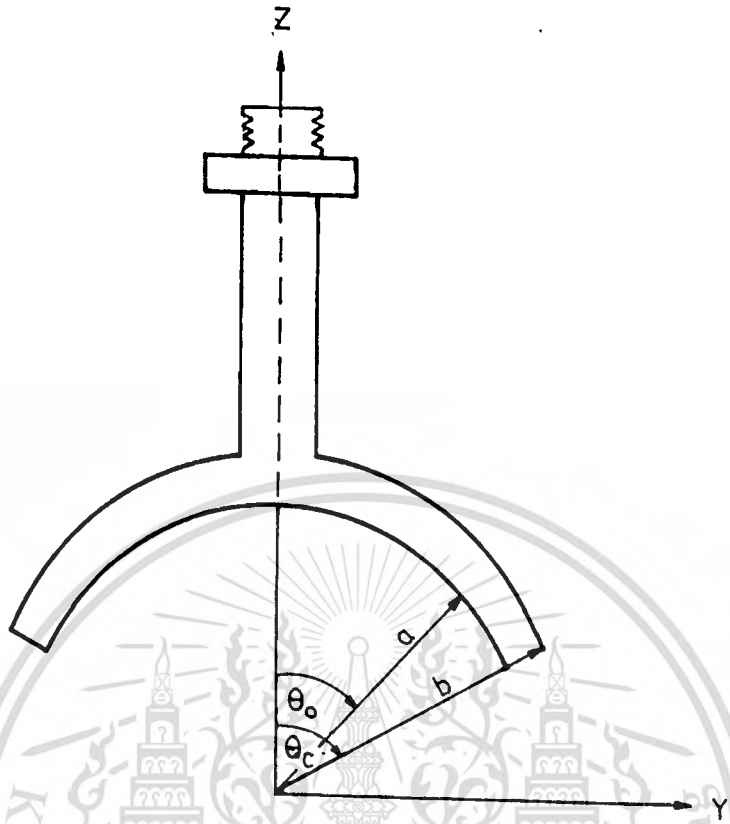

Fig.4.1 Concentric conducting spherical cavity

Let us consider E_r, E_θ and H_o the three components of the transverse magnetic spherical wave, TM_{mn} . These fields rely on a wave function ψ formed by the product of the following functions

$$T(r) = A\hat{J}_n(\beta r)+B\hat{Y}_n(\beta r) \qquad (4.10)$$

and

$$T(\theta,\phi)=[CP^m{}_n(\cos\theta)+DQ^m{}_n(\cos\theta)][(P\cos m\phi+Q\sin m\phi)] \qquad (4.11)$$

when β is the phase constant. $P^m{}_n$ denotes associated Legendre function, $\hat{J}_n$ and $\hat{Y}_n$ denote spherical Bessel's function of first kind and second kind, respectively. Coefficients

A,B,C,D,P and Q are determined from the appropriate boundary conditions. The azimuthal variation of these fields are function of trigonometric functions and a mode number "m". In order to force the field inside the cavity to be independent of ϕ, the mode number m must be zero and n must be an integer. There remains three components of the fields; E_r,E_θ and H_ϕ. For a specified resonance frequency, the fields inside the cavity will be satisfied by the boundary condition that tangential electric field at the conducting surface vanishes[27]:

$$P^m_n(\cos\theta)\big|_{\theta=\theta c} = 0 \qquad (4.12)$$

and

$$-B/A = \hat{J}'_n(\beta a)/\hat{Y}'_n(\beta a) = \hat{J}'_n(\beta b)/\hat{Y}'_n(\beta b) \qquad (4.13)$$

where prime denotes derivative with respect to r.

A conical angle θ can be derived from (4.12) and are shown in Table 4.1. The ratio of $\hat{J}'_n(\beta r)/\hat{Y}'_n(\beta r)$ are plotted for various values of βr and n as shown in Fig.4.2 in order to simplify the way to fix the solution of (4.13). According to the value of radius a is less than the value of radius b, therefore, at a specified value of $\hat{J}'_n(\beta r)/\hat{Y}'_n(\beta r)$ (or-B/A), the lower value of βr corresponds to βa while the higher one corresponds to βb. Employing (4.12) and (4.13) the cavity can be designed for a specified mode (TM_{0n}) and the field inside the cavity can be determined from (4.4) to (4.5c).

4.4 Numerical Results

It is evident from (4.11) that the field inside the cavity varies along the coordinate θ as a function derivative of associated Legendre function. From calculations, the position of the maximum value for each mode are found out as illustrated in Table 4.1. For a given value of resonance frequency, it is realized from Fig.4.2 that the spherical radii of the cavity in the higher mode will be longer than that of the lower mode cavity. It should be noted that the

conical angle decreases when the operating mode increases. It is also observed that resonance condition for any other higher mode cannot take place. Therefore all of energy is concentrated in the design mode. In order to compare Q-factors of various modes, they are calculated from [28]

$$Q = \frac{\omega_r W}{P_d} \tag{4.14}$$

where W is the energy stored in the cavity = $W_e = W_m = \frac{\mu \int_v |H|^2 dv]}{2}$

P_d is the power dissipated on the wall of the cavity = $\frac{Rs \oint_s J.J_s^* ds}{2}$

and Rs is the surface resistance of conductor

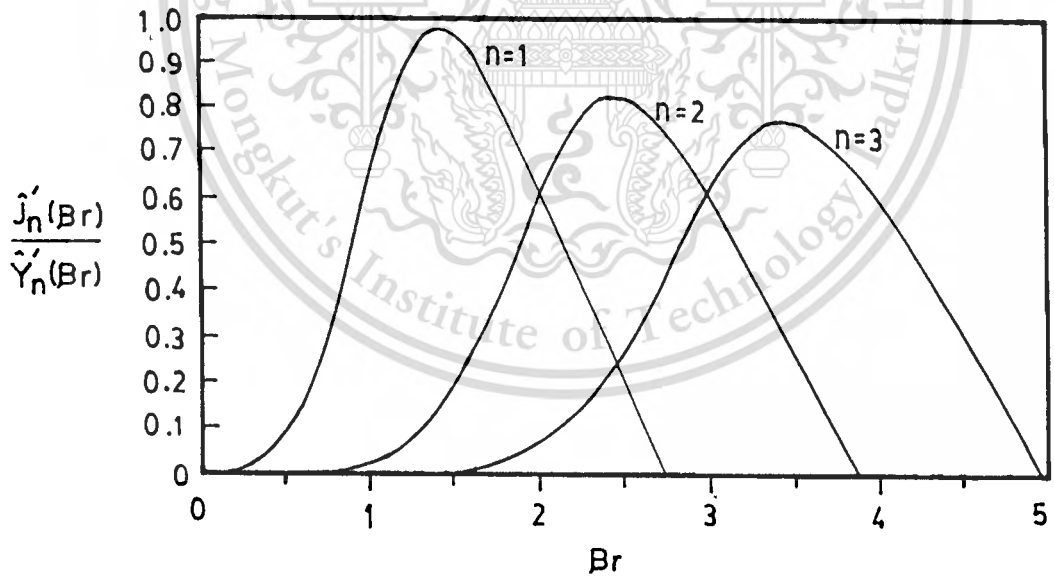

Fig.4.2 Characteristic of $\hat{J}_n'(\beta r)/\hat{Y}_n'(\beta r)$ versus βr

For a specified mode and resonance frequency, as the value of -B/A is decreased (this corresponds to the wider the different between b and a) the Q-factor will be increased. The maximum Q-factor will be obtained when -B/A vanishes as can be recognized from Table 4.1. It is noted that the maximum of Q-factor is increased as the operating mode is increased.

Table 4.1 Characteristics of the Cavity

n	$\theta_c(^0)$	$\theta_0(^0)$	βa	βb	-B/A	Q*Rs
1	90	90	1.29	1.55	0.943	41.98
			1.12	1.78	0.800	89.53
			1.05	1.89	0.711	107.19
			0.115	2.72	0.000	205.60
2	54.5	45	2.37	2.53	0.822	27.34
			2.19	2.74	0.756	80.26
			2.01	2.97	0.627	121.48
			0.60	3.87	0,000	220.60
3	39.6	36	3.37	3.56	0.762	32.32
			3.20	3.75	0.715	81.91
			3.00	3.99	0.608	127.88
			1.05	4.97	0.000	236.36

Rs:Surface Resistance of Conductor

4.5 Experimental Results

A TM_{02} mode cavity made of brass was fabricated to resonate at the frequency of 2450 MHz using -B/A equals to 0.756. The inner and outer radii are 4.3 and 5.3 cm, respectively, thereby a 54.5° conical angle was used. To excite the cavity, an electrical probe was protruded from a 50 ohms transmission line into the cavity and was varied until the lowest reflection coefficient

was observed. It is noted that the diameter of the probe should be the same as that of the coaxial line and the probe touches the other spherical surface. Reflection coefficient of the cavity was measured by using an HP8720C microwave network analyzer. Frequency was scanned from 2000 MHz to 2720 MHz and the lowest reflection coefficient which coresponds to the resonance occurs at 2360 MHz as shown in Fig.4.3. This corresponds to the design error of 3.67% which is practically acceptable. A Q-factor obtained from $f_0/\Delta f$ is 2620 which is 17% error from the calculation result of 3160. This would result from the present of the probe in the cavity. Moreover even we scanned the frequency up to 10 GHz (not shown) no other resonance occurs as expected.

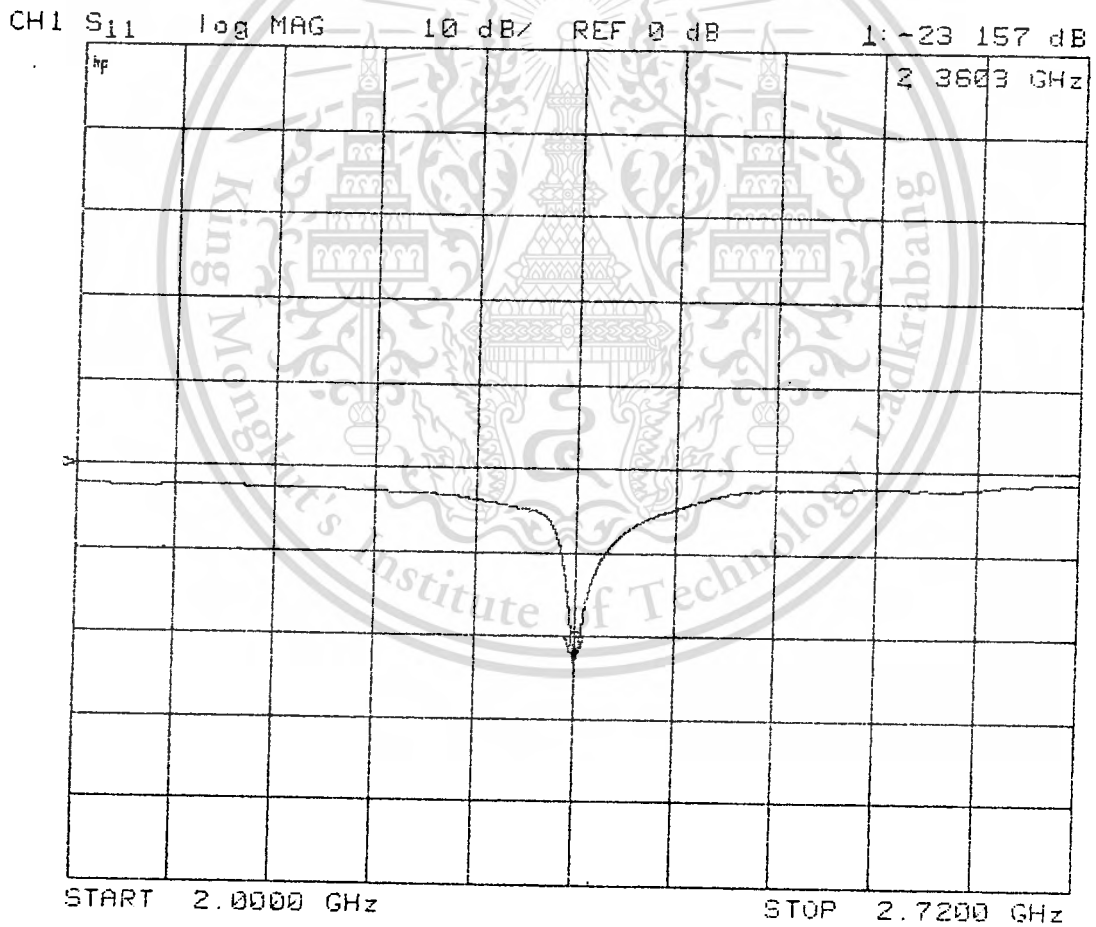

Fig.4.3 Frequency response of reflection coefficient

The other cavity was designed to resonate at 1000 MHz with -B/A equals to 0.805, θ_c=54.5^0 and a and b are 11.0 cm and 12.45 cm, respectively. On the outer spherical surface circular holes with diameter of 4 mm were drilled at the conical angles of 5,10,15, 20,25, 30, 35,40 and 45 degree. An electric field probe made of a semirigid coaxial cable was used to sample the radial component of electric field (E_r) in the cavity. The measured results were plotted and compared to those from calculation as illustrated in Fig.4.4. It is obvious that they are in acceptably good agreement.

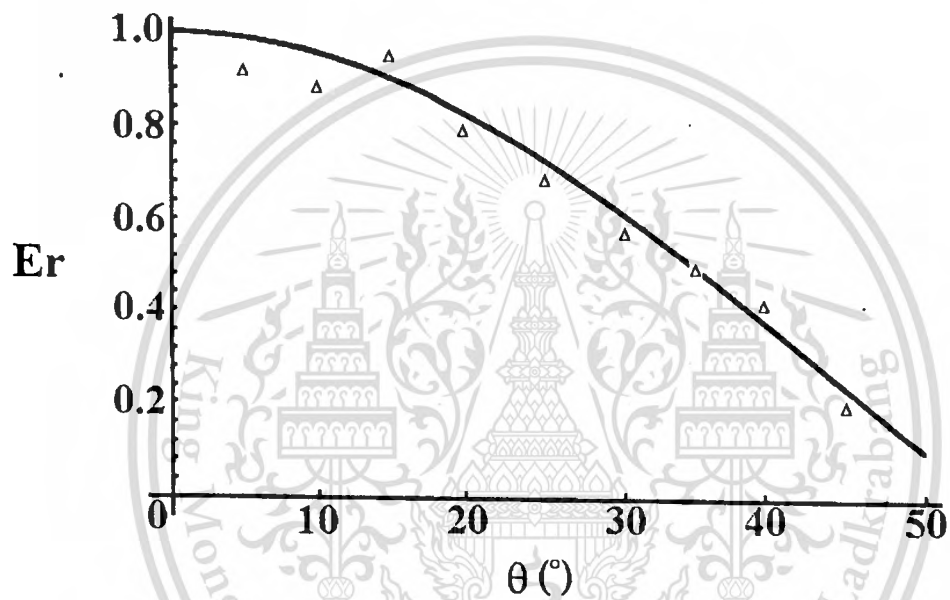

Fig.4.4 Measured electric field inside the cavity

4.6 Conclusion

A concentric conducting spherical cavity is described, and the field inside has been analyzed. It is revealed that the Q-factor of the cavity can be varied by using the different size of the cavity. From the result in Table 4.1 it is realized that the cavity with the wider radii seperation possesses a higher Q-factor. The higher the operating mode the higher the Q-factor. This cavity will be applied as a means to excite a slot array as will be shown in the next chapter.

Chapter 5
Concentric Conducting Spherical Cavity-Backed Slot Array Applicator

5.1 Introduction

This chapter is associated with a concentric conducting spherical cavity-backed slot array applicator. The configuration of the applicator which is an array of slots on an inner surface of a concentric conducting spherical cavity, is described. Then SAR distributions from some specific applicators are illustrated. In order to design a focus applicator, a water bolus is used to eliminate undesired hotspots.

5.2 Focus Array

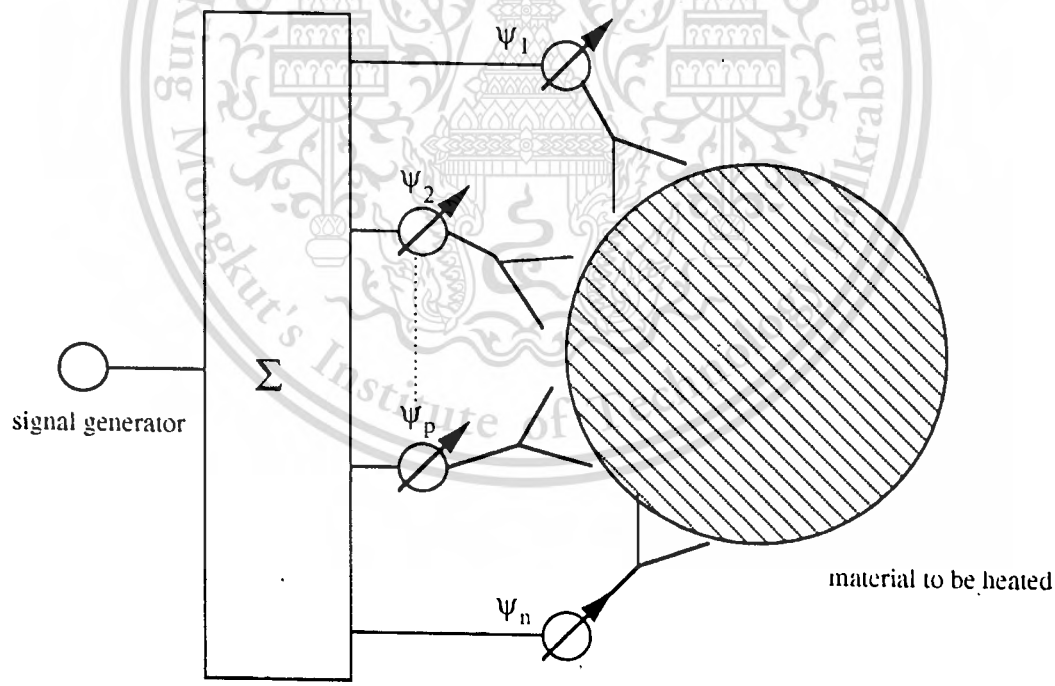

Fig.5.1 Focus array

To produce a field focused at a point in a medium, the field contributions from each radiator should be inphase at that point. Then, to obtain a focus of the fields from every radiator, on the spherical surface, at the center of the sphere as shown in Fig.5.1, the following condition must be held[11].

$$\frac{2\pi a}{\lambda} + \psi_p = \text{constant} \qquad (5.1)$$

where λ is the wavelength of fields in the medium, a is a radius of the sphere and ψ_p (p=1,2,..,n) denotes phase of excitation fields at the radiators.

5.3 Concentric Conducting Spherical Cavity-Backed Slot Array Applicator

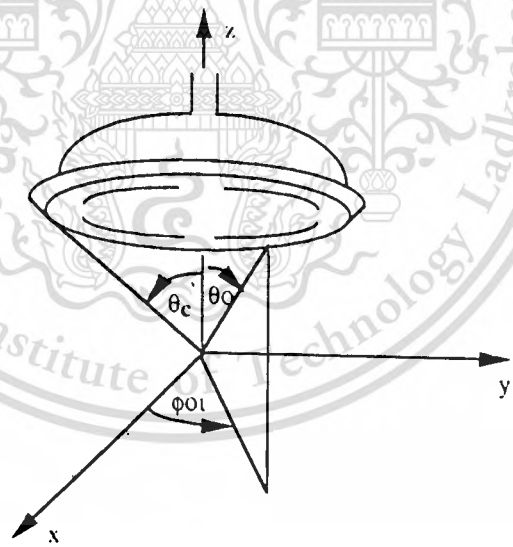

(a) Perspective view

Fig.5.2 Concentric conducting spherical cavity-backed slot array applicator

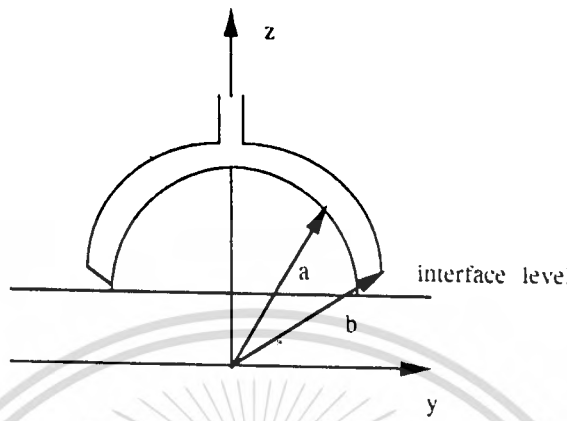

(b) Side view

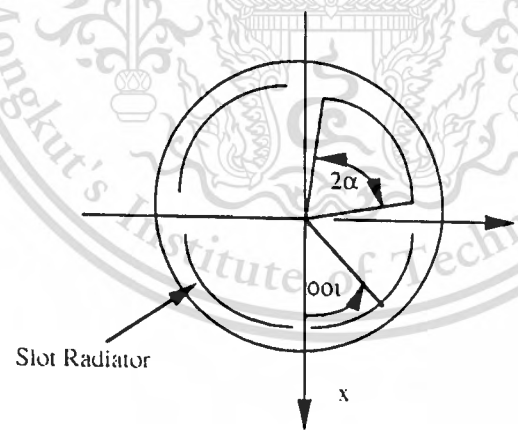

(c) Bottom view

Fig.5.2 (cont'd)

The proposed hyperthermia applicator consists of a concentric spherical cavity as shown in Fig.5.2(a), which is used to excite an n-slot array as radiators. The cavity is excited in TM_{mn} mode by a coaxial cable with the inner conductor that protrudes into it. The inner and outer spherical radii of the cavity are a and b respectively as shown in Fig.5.2(b). Both spherical conductors are enclosed by a conical conductor at an angle $\theta=\theta_c$. The slot radiators are cut on the inner spherical conducting surface along the line with angle $\theta=\theta_o$, along which the surface current density is predicted to be maximum. This position can be found by calculating the field component of E_θ as a function of θ in (4.4)-(4.4c). In Fig.5.2(c), ϕ_{oi}'s are supposed to be the center of the *i th* slot (i=1,2,...,n).

It is evident from (5.1) that ψ_p should be identical, namely, each slot has to be inphase excited. Fortunately it is possible to force the field strength inside the cavity to be the function that is independent from the azimuthal angle ϕ, and this means that every slot radiator can be excited by equal field strength. It can be accomplished by exciting the cavity in TM_{on} mode.

Recalling that the field has the same phase at the same conical angle θ, the slots are to be cut horizontally along an azimuthal plane of the sphere at the positions of the same angle θ_o so as to produce inphase excitation to each radiator. It is evident that the total length of the slots are limited by the circumference of the sphere at the conical angle θ_o minus the spacings between the slots. For the sake of simplicity for field expressions, a slot length is expressed as a function of angle α as shown in Fig.5.2(c).

5.4. SAR Distributions

An applicator of a slot array can be designed to operate in several modes (TM_{on}). Each of them possesses different characteristics and dimensions. It is essential to consider about an acceptable size of the cavity to be an excitor. The dimensions of the two-slot applicators excited by three modes TM_{01},TM_{02} and TM_{03} can be obtained from (4.10)-(4.13) at 2450 MHz, and are shown in Table 5.1.

Table 5.1 Theoretical Performance of Two-Slot Applicators

mode	a(cm)	b(cm)	θ_c(°)	θ_o(°)	2α(°)	Penetration Depth from the Interface (cm)	EFS of the Desired Hotspot(cm^2)
TM_{01}	2.18	3.47	90.0	90.0	178	0.5	0.4
TM_{02}	4.30	5.30	54.5	45.0	178	2.7	1.0
TM_{03}	6.23	7.31	39.6	31.0	178	0.4	-

By computer simulations, SAR distributions of these applicators are shown in Fig.5.3. It is noted that the maximum of SAR appears near the slot surfaces and decreases along the path out of the slots. The penetration depth can be estimated from the definition; a depth at which SAR reduces to 13.5% [10]. Fig.5.3(a) illustrates that an applicator made from a TM_{01} cavity has an ability to focus an electric field at the center of the spherical cavity. The EFS of the desired hotspot is approximately 0.4 cm^2. However for an applicator made of a TM_{02} cavity which has an inner spherical radius 4.3 cm only, the center of the sphere is at the depth of 2.5 cm from the horizontal interface level as shown in Fig.5.3(b). It is found that in this case the EFS is around 1 cm^2, which is desirable for a local heating because heat can be confined in a remarkably small area. It can heat a tumor without burning surrounding healthy tissue. By contrast from the SAR distribution of an applicator made of a TM_{03} cavity in Fig.5.3(c), focusing capability is not noticable.

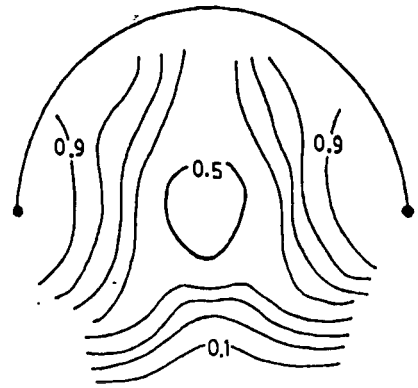

(a) TM_{01} applicator

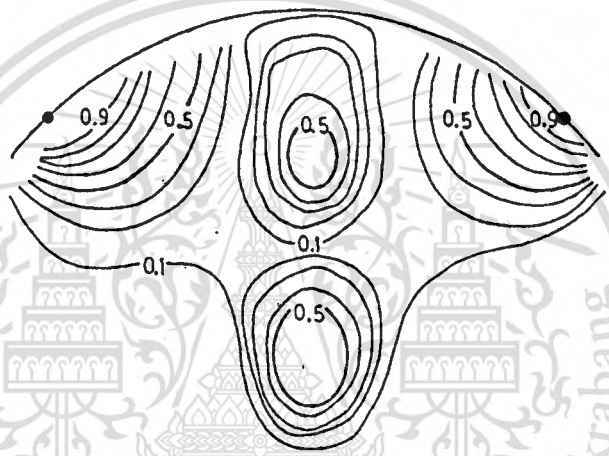

(b) TM_{02} applicator

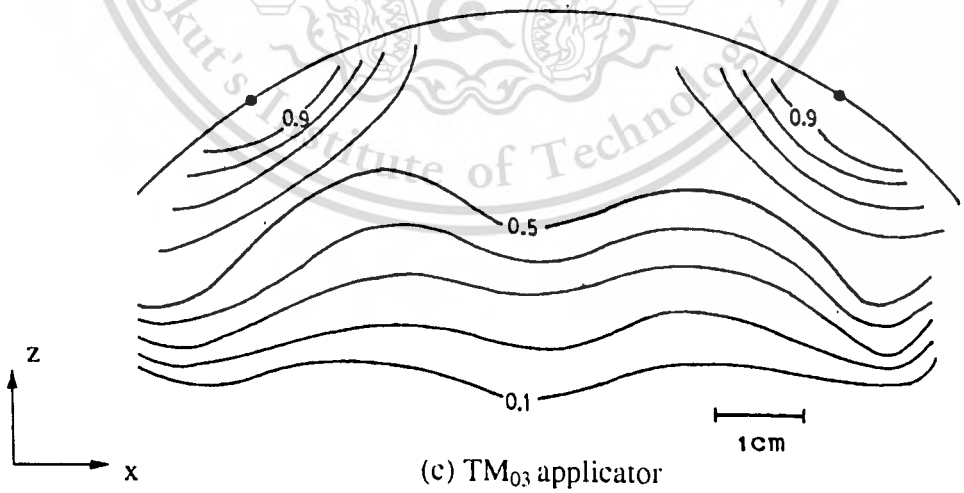

(c) TM_{03} applicator

Fig.5.3 SAR distribution

5.5 Bolus Design

According to the SAR distribution displayed in section 5.4, it is realized that the applicator made of the TM_{02} mode cavity is suitable for focusing the electric field deepen into the heated medium. In addition to the desired hotspot at the center of the sphere, there are undesired hotspots next to the slot apertures. These undesired hotspots may raise the temperature of the skin to an excessive temperature so that it may burn out. Therefore, in practical we have to eliminate such hotspots and we expect to accomplish by using a water bolus which performs convection at the interface between the heated medium and the applicator. One of usable geometry of the bolus is depicted in Fig. 5.4.

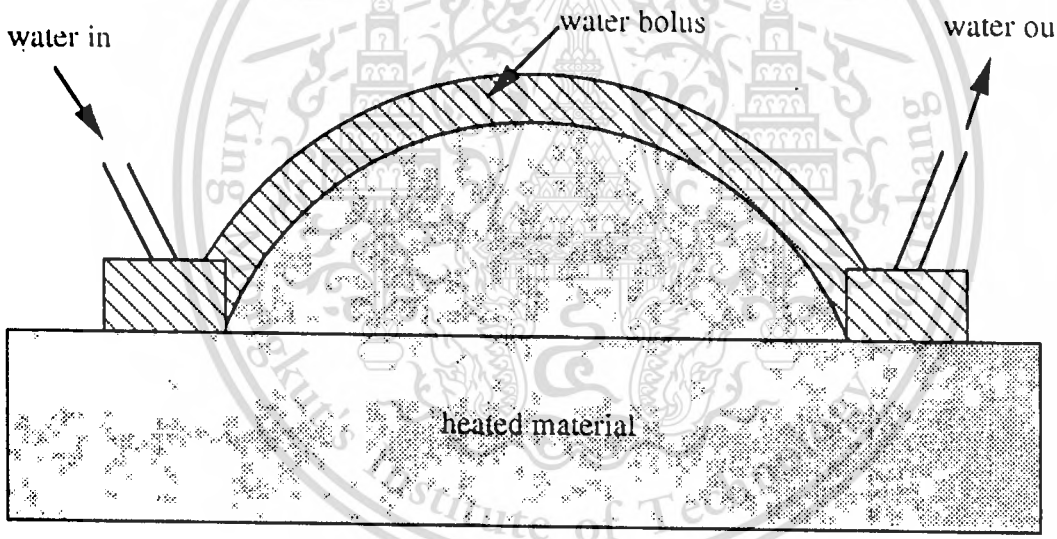

Fig.5.4 Geometry of water bolus

For reference study, the two dimensional conduction heat equation is solved numerically by using the finite difference method. The equation is expressed in cartesian coordinate system in

order to show the resultant temperature distribution in the form of regtangular grid which can be understood easily. This equation is shown as follows[29]

$$\frac{\partial^2 T}{\partial x^2} + \frac{\partial^2 T}{\partial z^2} + \frac{q}{k} = 0 \qquad (5.2)$$

where q is heat source (w/m^2)

k is thermal conductivity ($w/m^{\circ}C$)

and T is temperature ($^{\circ}C$)

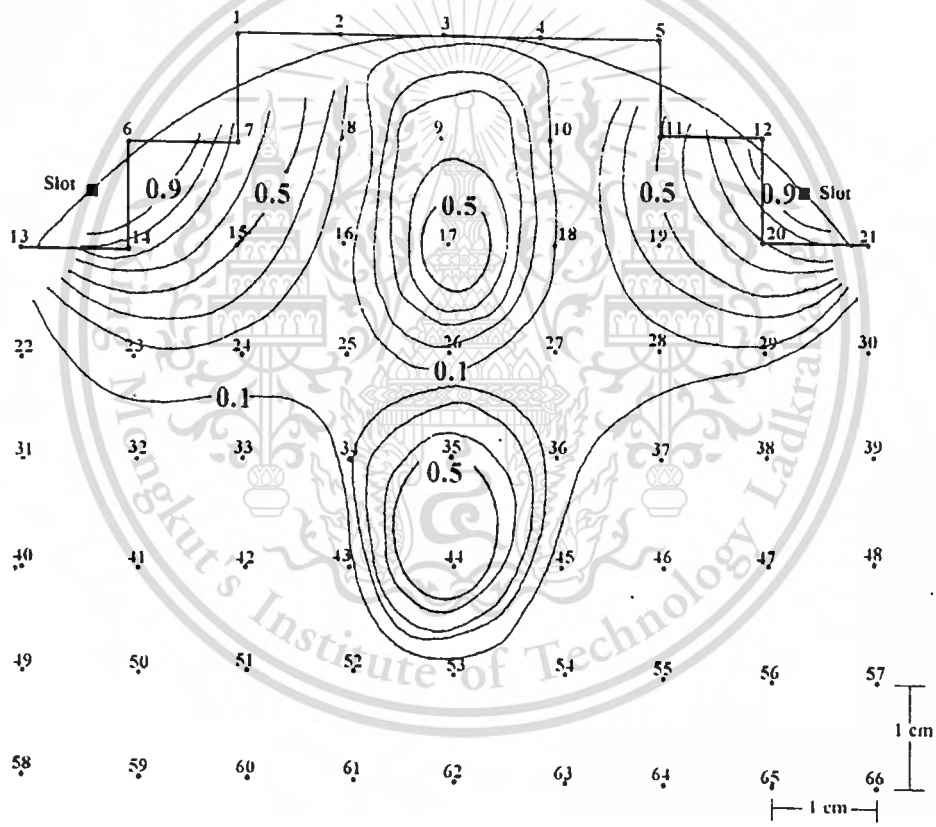

Fig.5.5 Geometry of finite difference heat transfer equation

The region of interest is divided into nodes with equal seperations (Δl) of 1 cm, as shown in Fig.5.5. The numbers displayed at each point in Fig.5.5 indicates the number of nodes

temperature to be calculated. The interior nodes are subjected to the heat source q from the SAR distribution from the result of section 5.4. The number on the SAR contour shows the relative magnitude of heat source (q). For these nodes, the geometry of the nodes can be illustrated in Fig.5.6(a) and the corresponding finite difference equation is

$$T_{m+1,n}+ T_{m,n+1}+ T_{m-1,n}+ T_{m,n-1}- 4T_{m,n} +\frac{q}{k} (\Delta l)^2 = 0 \qquad (5.3a)$$

The nodes on the boundary between the medium and the applicator are predetermined subject to the convection boundary condition. The geometry of these nodes is shown in Fig.5.6(b), Fig.5.6(c) and Fig.5.6(d), respectively. The finite difference equation of the nodes in Fig.5.6 (b) is obtained as follow

$$\frac{h\Delta l T_\alpha}{k}+ \frac{1}{2}(2T_{m-1,n}+ T_{m,n+1}+ T_{m,n-1})- \frac{(h\Delta l+ 2)}{k} T_{m,n}= 0 \qquad (5.3b)$$

whereas the equation of the nodes in Fig.5.6(c) is

$$\frac{2h\Delta l T_\alpha}{k}+ (T_{m-1,n}+ T_{m,n-1}) - \frac{(h\Delta l+1)}{k}T_{m,n} = 0 \qquad (5.3c)$$

and the equation of the nodes in Fig.5.6(d) is

$$\frac{2h\Delta l T_\alpha}{k} + 2T_{m-1,n} + 2T_{m,n+1} + T_{m+1,n} + T_{m,n-1} - \frac{2(3+h\Delta l)}{k}T_{m,n} =0 \qquad (5.3d)$$

In equations (5.3b),(5.3c) and (5.3d)

T_α is water temperature ($^\circ$C)

and h is convection heat transfer coefficient (w/m^2.$^\circ$C)

The convection heat transfer coefficient is the product of flow and heat capacity of water (cal/cc.$^\circ$C). For the nodes in the remainder of the medium temperature is kept constant at human temperature of 37 $^\circ$C.

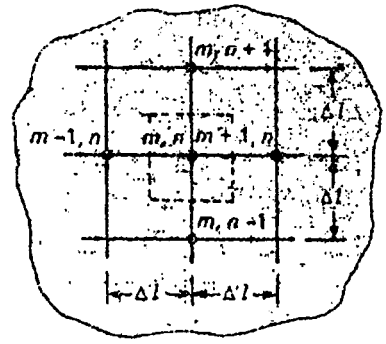

(a) Interior node

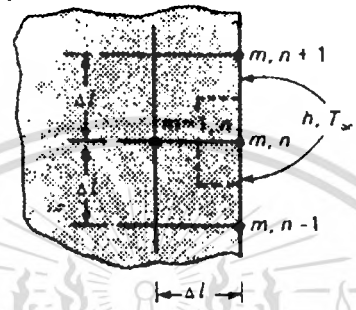

(b) Convection boundary node

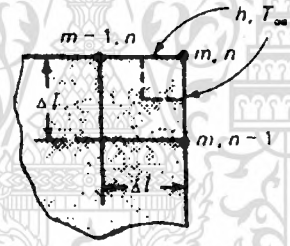

(c) Exterior corner with convection boundary

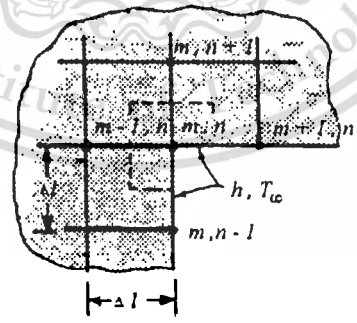

(d) Interior corner with convection boundary

Fig.5.6Summary of nodes for finite difference calculation

The apparent nodes are shown inFig.5.6(c). The corresponding equations are arranged in a matrix form and are solved simultaneously so that the temperature at the specified nodes are obtained. It is seen from these equations that the parameters which influence the temperature distribution are the convection heat transfer coefficient (h), the magnitude of heat source (q) and the water temperature (T_α). It should be reminded that the magnitude of heatsource is proportional to SAR and SAR is proportional to the square of electric field intensity. We investigate the way to cool the hotspots next to the slots down by controlling h (which means varying the speed) and the temperature of the water and the results are shown in Fig.5.7 to Fig.5.13. The number at a specific point in the following illustrations indicates the calculated temperature.

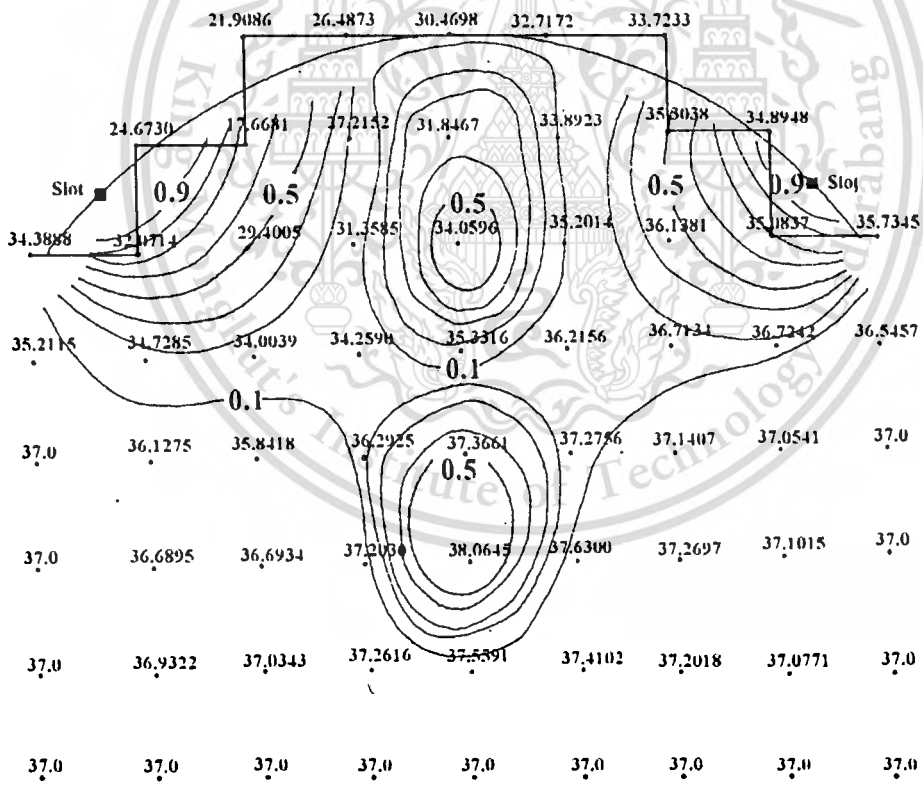

Fig.5.7 Temperature distribution when h=0.001w/m^2.°C,

Fig.5.7 shows the temperature distribution when h=0.001w/m^2.°C, T_a=5°C and q=50w/m^2. It is observed that when the magnitude of heat source (q) is low, we can not elevate the temperature up to a hyperthermic temperature (43-50°C). Then the magnitude of heat source q is increased to 100 w/m^2 and the temperature distribution is shown in Fig.5.8.

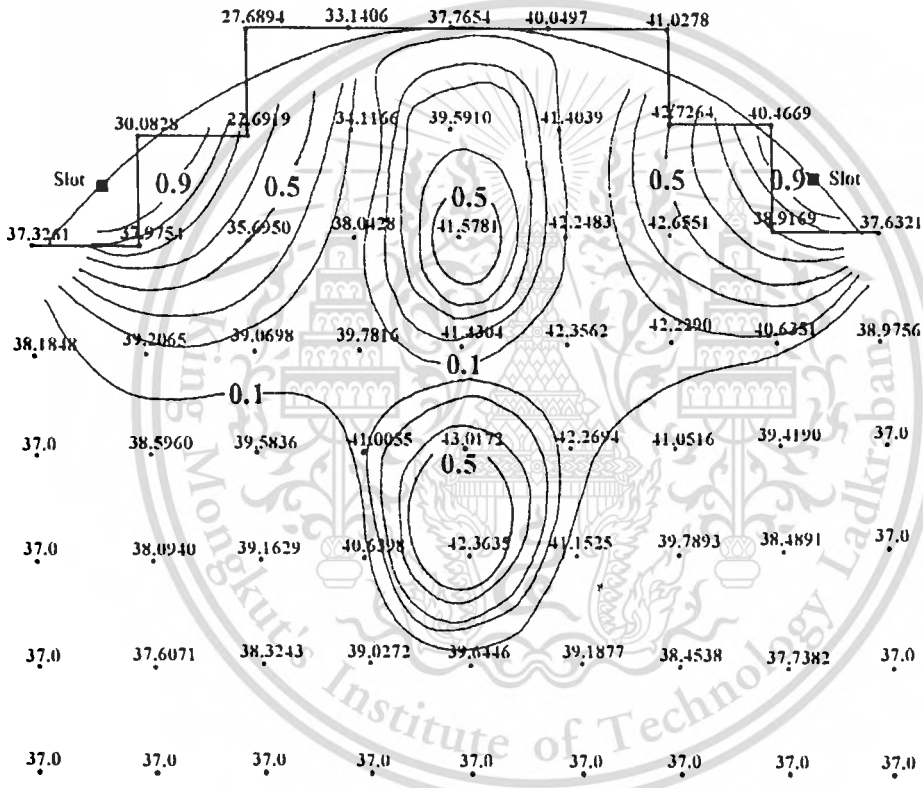

Fig.5.8 Temperature distribution when h=0.001w/m^2.°C, T_α=5°C and q=100w/m^2

In this case temperature at the focusing point is increased to 43.0°C. As we keep on increasing the magnitude of heat source q to 200w/m^2, it is found that the temperature is increased over the hyperthermic temperature as illustrated in Fig.5.9.

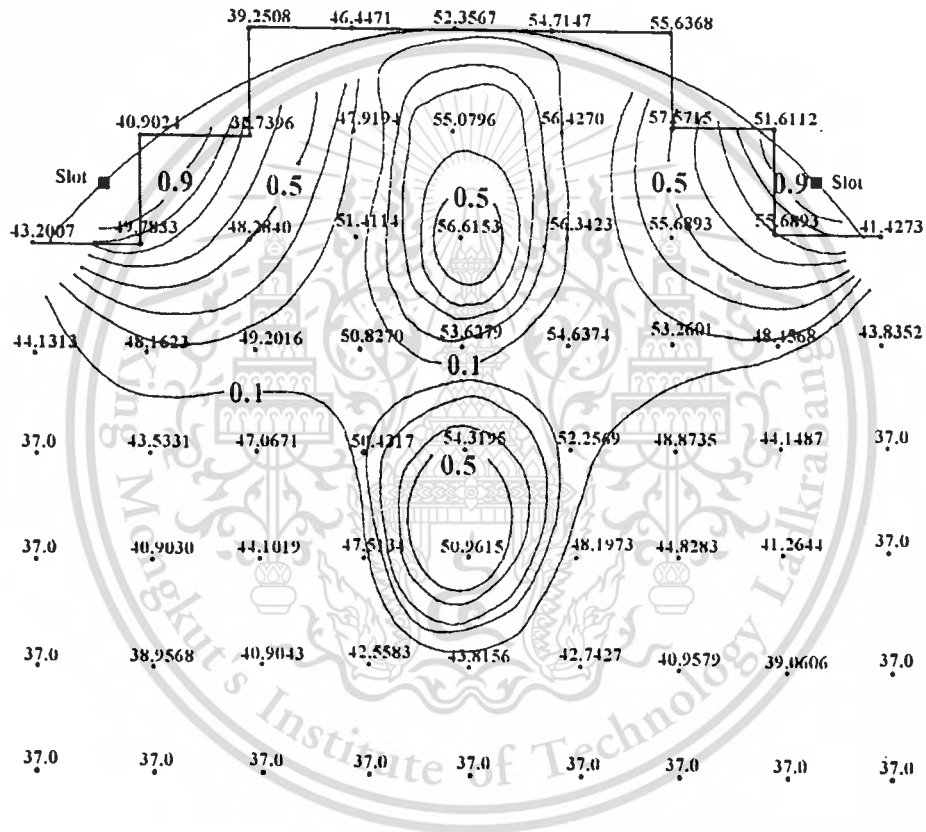

Fig.5.9 Temperature distribution when h=0.001w/m^2.°C,
T_α=5°C and q= 200w/m^2

Let us move back to investigate the temperature ditribution in Fig.5.8. Although the temperature at the focusing point is in the hyperthermic range, however, the region next to the right slot is increased to the temperature as high as 42.7°C. This signifies the undesirable hotspot. In order to eliminate this undesirable hotspot, we increase the convection heat transfer coefficient, $h=0.01 w/m^2.°C$, and observe the temperature distribution which is displayed in Fig.5.10. It is obvious from Fig.5.10 that as the convection heat transfer coefficient is increased, this can be realized by increasing the speed of water and the water bolus can eliminate the undesirable hotspot efficiently. However, the temperature at the focusing point has been a little bit reduced. We proceeded the investigation by increasing heat source up to $150 w/m^2$ while keeping $h=0.01 w/m^2.°C$ and $T_\alpha=5^{C}C$. Fig.5.11 shows the temperature distribution of such condition which is satisfactory. The temperature at the focusing point deepen into the heated medium is elevated to a hyperthermic temperature whereas the one in another part especially in the region next to the slots are cooled down. There remains only a desirable hotspot at the focusing point. It is noteworthy that the lower the water temperature the better the cooling action. However, in practical application, the patient might feel uncomfortable if the skin is too cold. Fig.5.12 shows the result that as the water temperature is increase to 10°C the desirable focusing characteristic still remains. But the temperature at the focusing point in addition to the surface can be increased. However, if the water temperature is increased to 20°C the surface temperature might be too high as illustrated in Fig. 5.13.

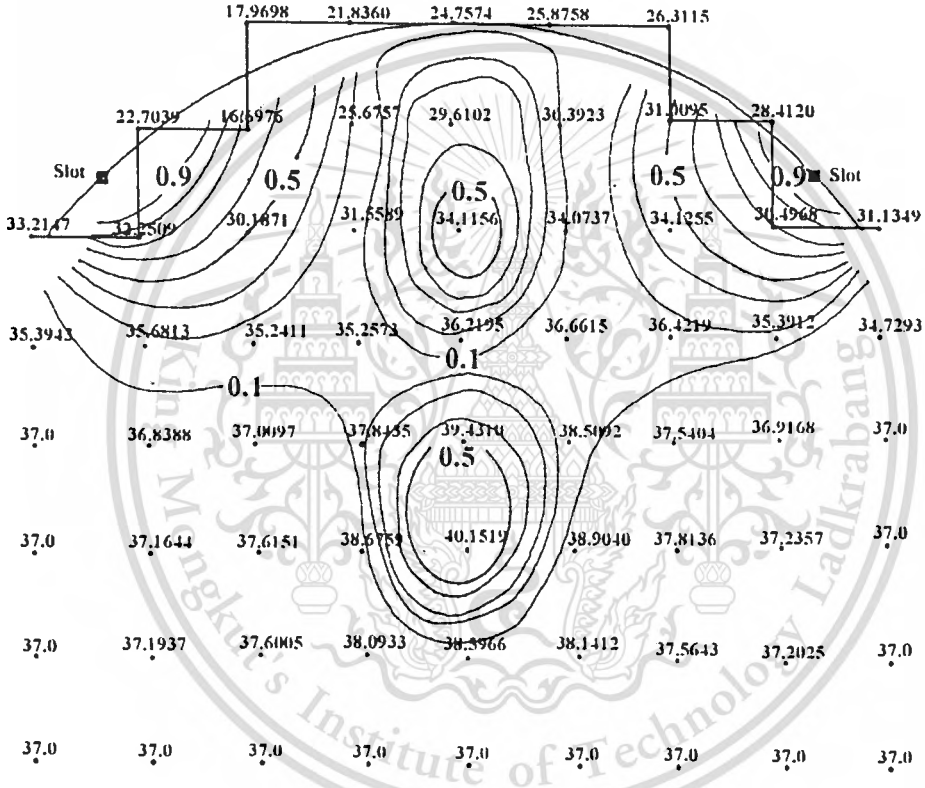

Fig.5.10 Temperature distribution when h=0.01w/m^2.^{o}C,

T_α=5^{o}C and q=100w/m^2

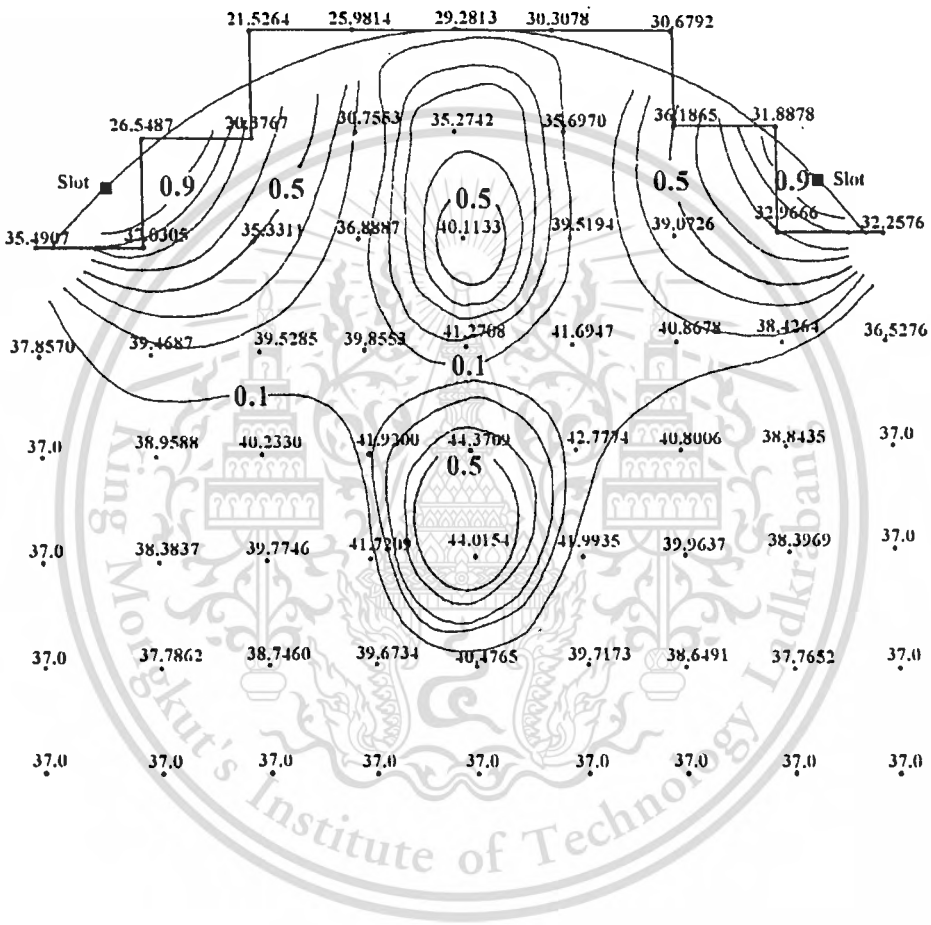

Fig.5.11 Temperature distribution when h=0.01w/m^2.^{o}C,

T_α=5^{o}C and q=150w/m^2

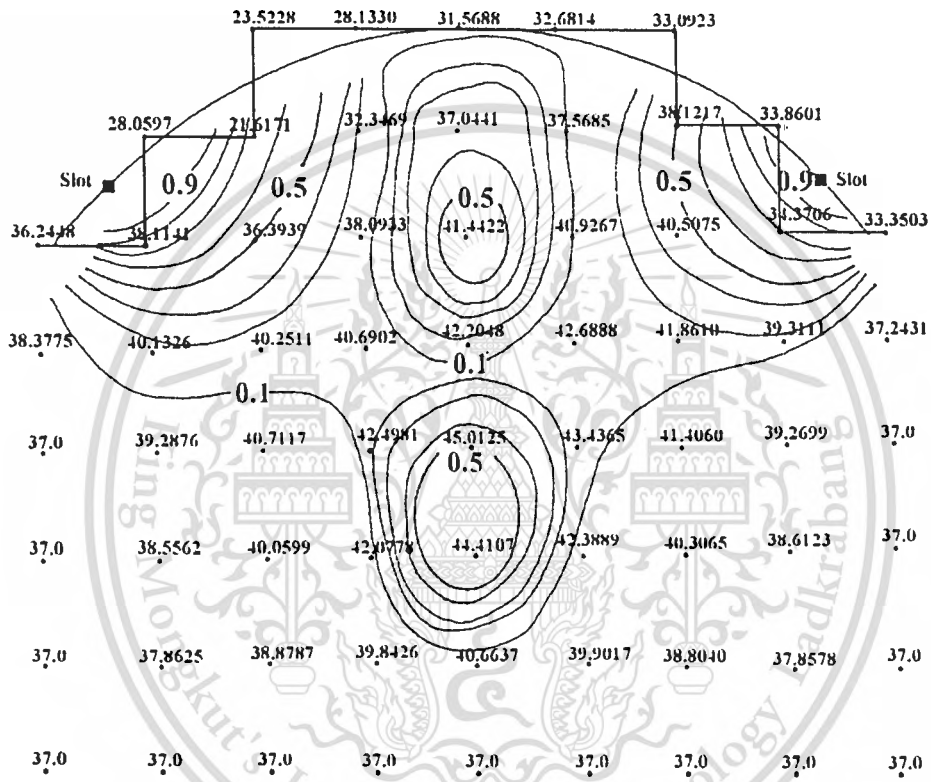

Fig.5.12 Temperature distribution when $h=0.01 w/m^2.°C$, $T_\alpha=10°C$ and $q=150 w/m^2$

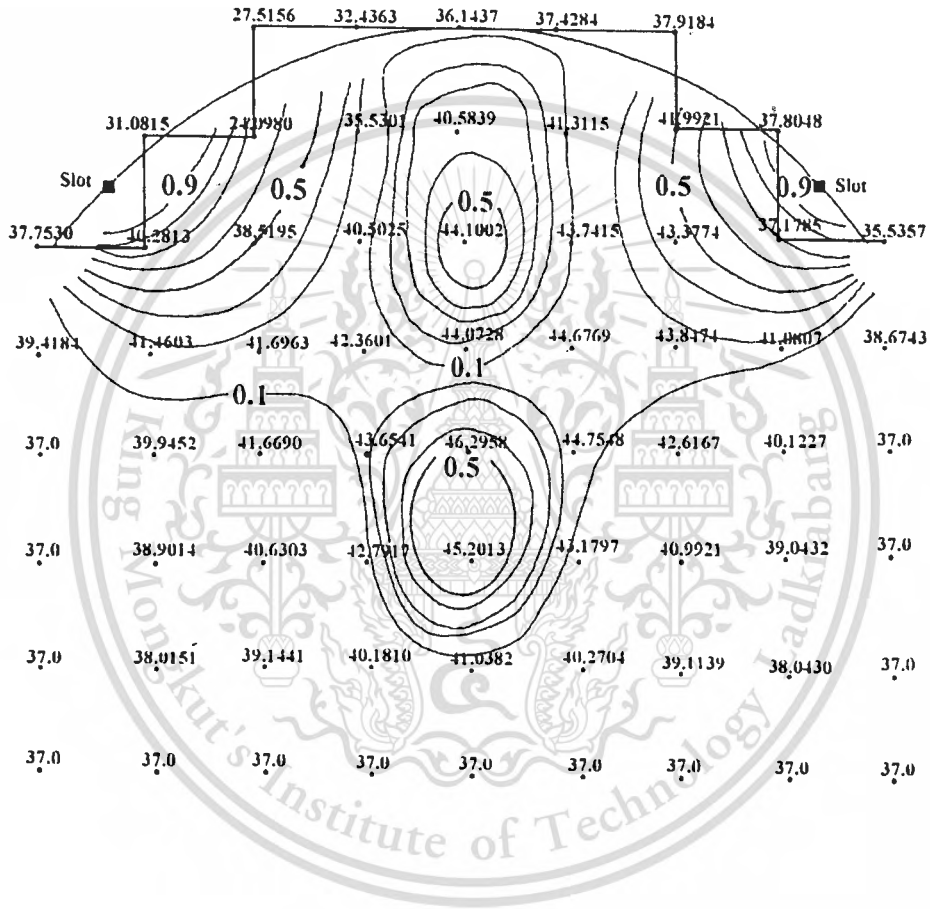

Fig.5.13 Temperature distribution when h=0.01w/m^2.°C,

Ta=20°C and q=150w/m^2

In case of the flat surface medium, the bolus has to be a water bag of which shape adequately fills the space between the applicator, as shown in Fig.5.14, and the cooling material should posseses electrical property similar to that of the heated material, i.e. it has ε_r

similar to the heated material, and has low conductivity so as to keep loss in this material as low as possible.

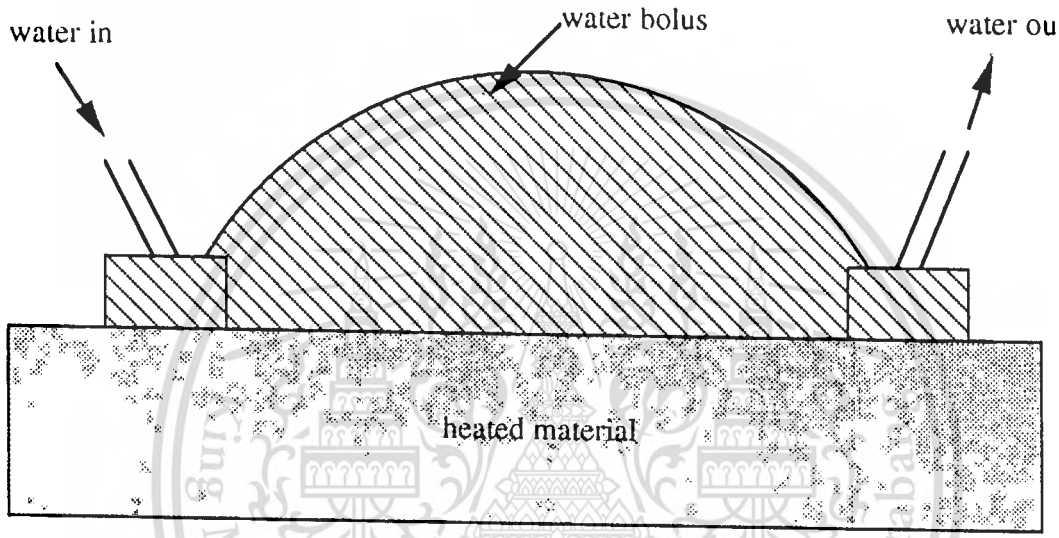

Fig.5.14 Geometry of a flat bolus

The reason why ε_r should be close to those of the heated material, is to reduce a reflection coefficient of the traveling field in the space [26].

5.6 Conclusion

It is concluded that in order to focus electric field deepen into a lossy material such as human muscle, a TM_{02} cavity is the most suitable to feed the slot array. It is noticable that the number of slots in the applicator have the effect on EFS of the hotspot. The undesirable hotspot can be eliminated by using an appropriate bolus.

Chapter 6
Performance of The Applicator

6.1 Introduction

As the consequences of the materials in the previous chapter, the experiments have been established. Four applicators with TM_{02} cavities at 2450 MHz are realized; there are one-slot, two-slot, three-slot and four-slot applicators, respectively. The details of the experiments will be appeared in this chapter.

6.2 Radiation Patterns

A particular clinical requirement for which the spherical applicator may be suitably applicable is to locally heat a tumor in the spherical part of human body such as breast or head, etc.. Fig.6.1 shows the field mapping arrangement [30] used to measure radiation patterns of the applicators ; one-slot and two-slot and three-slot applicators, in our experiments.

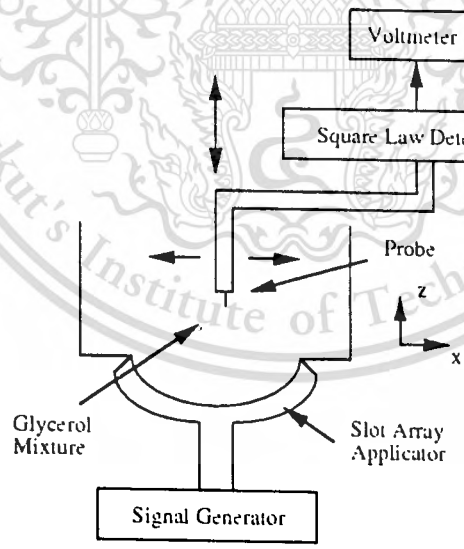

Fig.6.1 Field mapping arrangement

In this figure the water broad-mounted container with a spherical bottom is placed on the surface of the applicator. The inner and outer radii of the cavities of the applicators are 4.3 cm and 5.3 cm, respectively. The slot locations are in the direction of θ_o=45° . Since the circumference of the sphere at such angle is 19.0 cm, each slot length of 9.25 cm is chosen and the spacing between the slots is 2.5 mm for two-slot applicator. The photograph of the two-slot and three-slot array applicators that were designed to operate at 2450 MHz is shown in Fig.6.2.

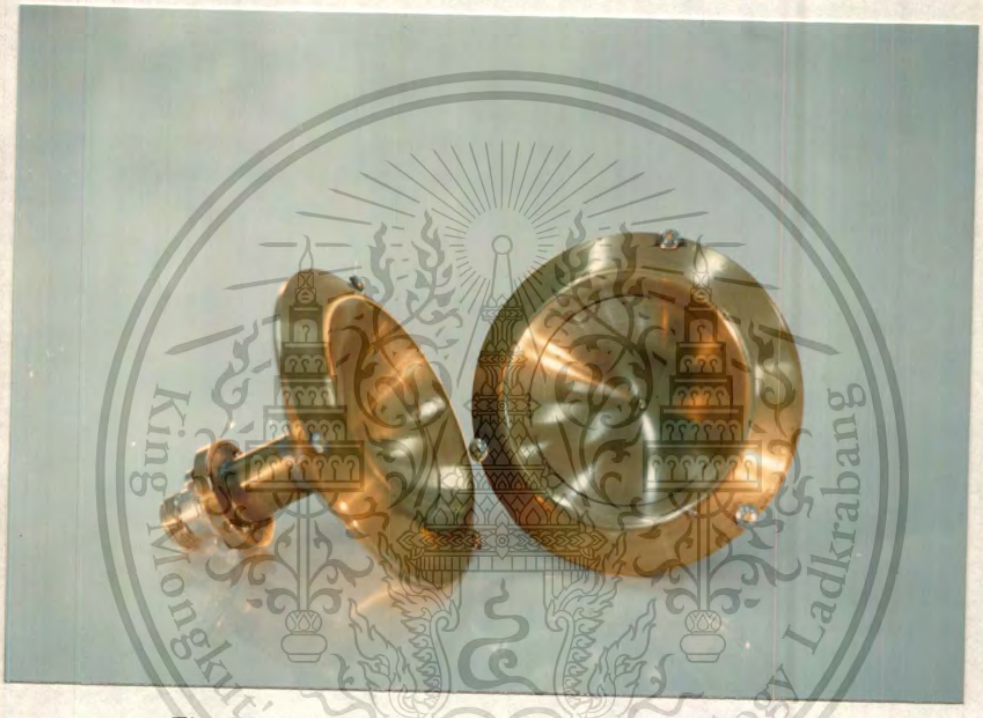

Fig.6.2 Photograph of the applicators in the experiment

A 3.5 mm long electric field probe was moved on the x-z plane, as refer to the reference coordinate in Fig.6.1, to measure the distribution of squared electric field intensity in phantom prepared from glycerol and water (30:70 by weight) to simulate a human muscle. Field patterns which are measured on x-z plane are shown in Fig.6.3.

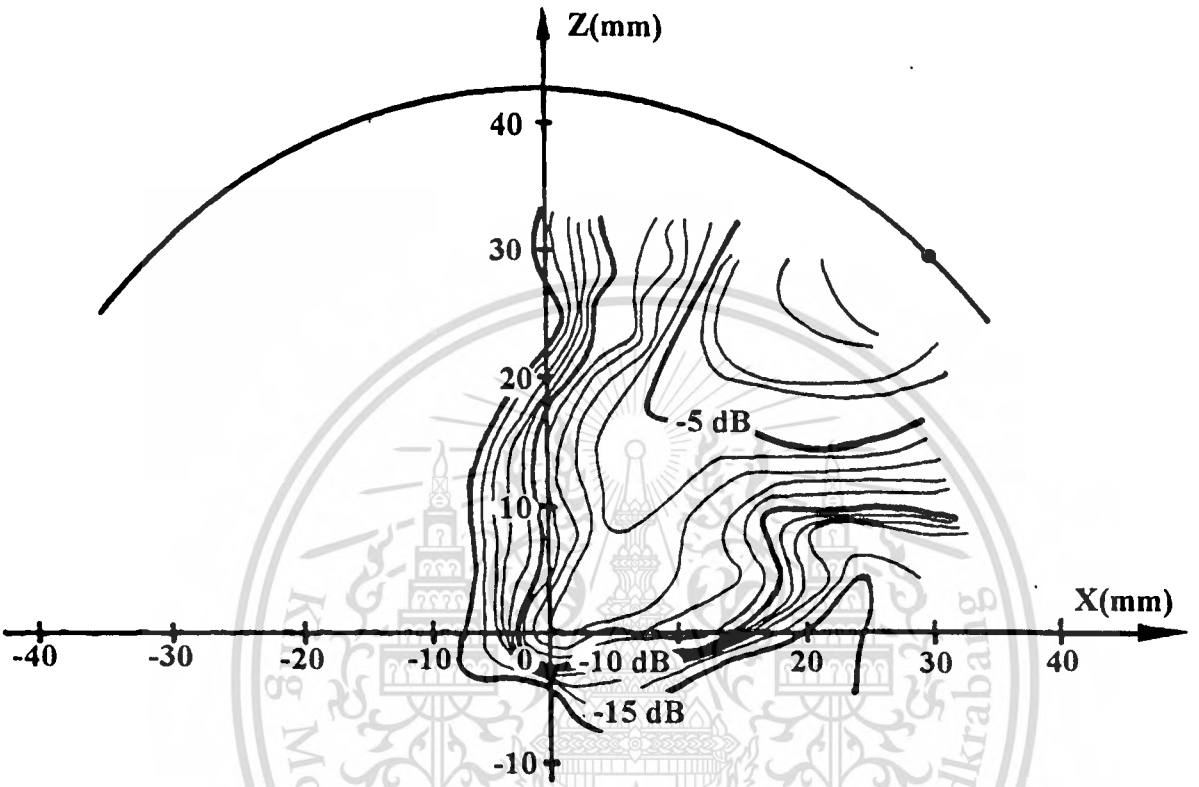

(a) one-slot applicator

Fig.6.3 Field pattern of the experimental applicators

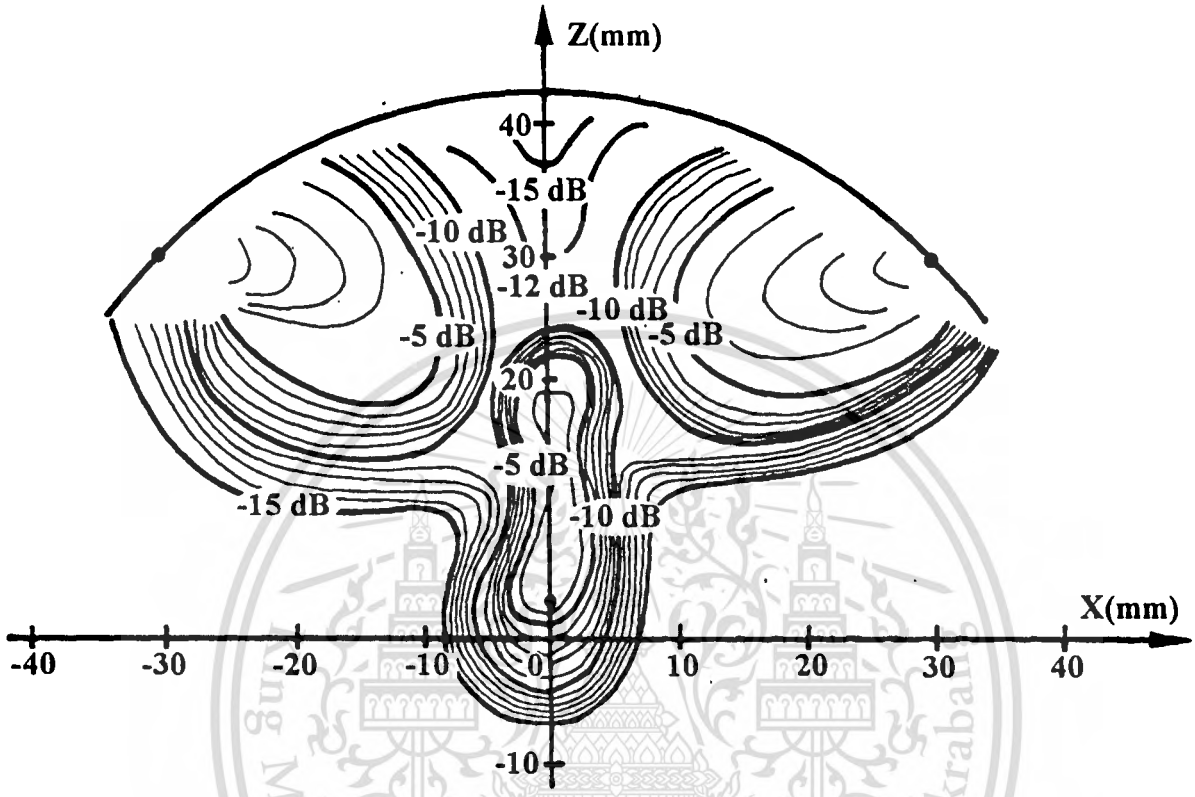

(b) two-slot applicator

Fig.6.3 (cont'd)

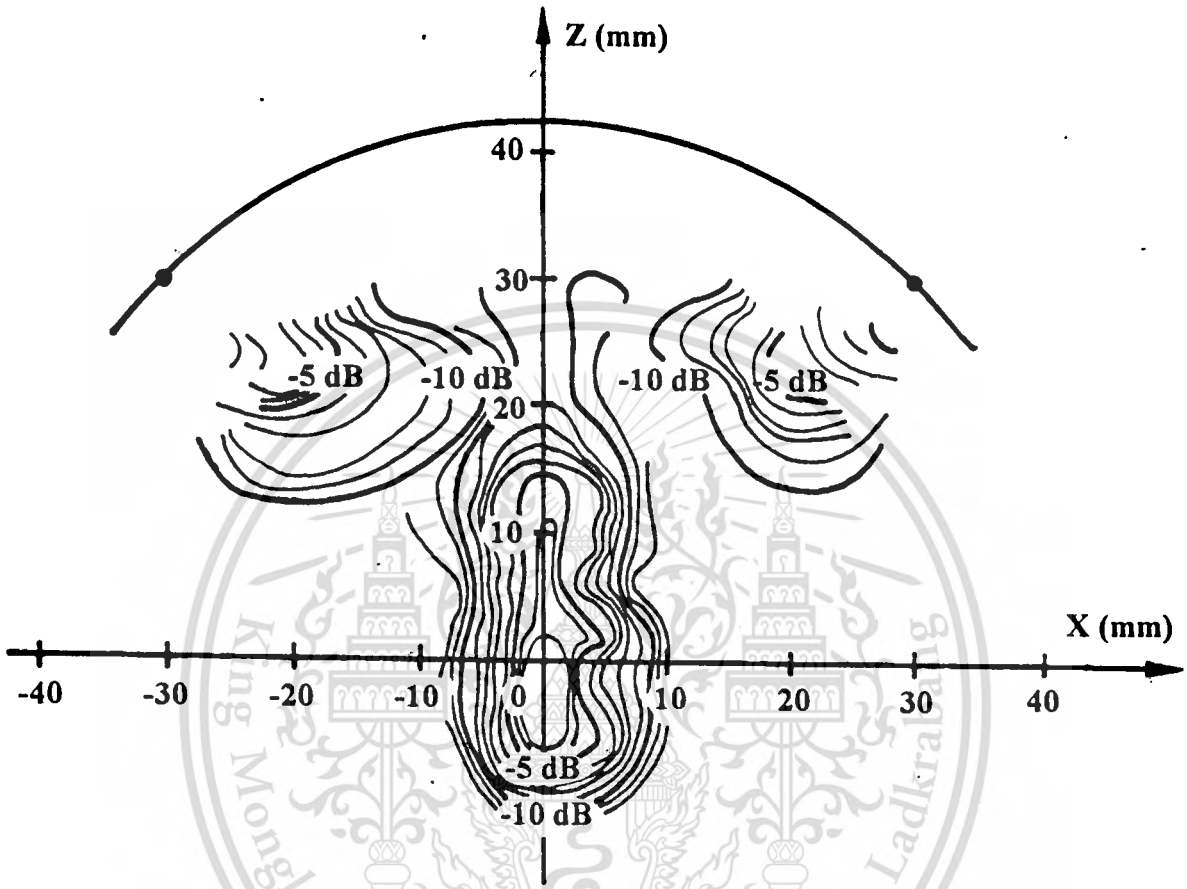

(c) three-slot applicator

Fig.6.3 (cont'd)

Fig.6.3(a) shows the field pattern for the one-slot applicator, it is seen that the square of electric field intensity has its maximum at the slot and its amplitude decreases along the distance. A contour of -8.68 dB which correspond to a penetration depth (SAR=13.5%) is around the center of the sphere which is 2.5 cm from the interface level. For the two-slot applicator, as shown in Fig.6.3(b), there are some differencesfrom Fig.6.3(a), the contour of -6dB passes the center and the energy is 2 dB higher than that of the one-slot applicator. It is observed that there is an additional hotspot around the center. The spotsize is defined as the area surrounded by a -3 dB contour down from the value at the center (-9 dB contour). The hotspot appears deep inside the heating material in addition to the two spots near the slots. The width of this spot is about 1 cm. A field pattern of the three-slot applicator is illustrated in Fig.6.3(c). The desirable hotspot at the center is remarkable. The maximum value at the center is around -3 dB and the hotspot size (-6 dB) is almost the same as that of the two-slot applicator. However, the penetration depth is longer. From this investigation it is realized that an appropriate cooling water bolus must be designed to cool down the heat near the surface and its shape should be a spherical shape which conforms to the surface of the applicator. The material filled in the bolus should be the cold low loss material with dielectric constant which is close to that of the human muscle in order to maintain the field matching condition.

6.3 Input Impedance

An input impedance is an important parameter associated with power transmission from a source via an applicator to a material to be heated. Therefore, an input impedance of an applicator must be examined when it is attached to a muscle phantom. Experiments were made by using an HP 8720C Microwave Network Analyzer to measure an impedance of three applicators as shown in Table 6.1. The results are plotted on the Smith Chart as shown in Fig.6.4. When these three applicators are directly contact with the human muscle phantom which dielectric constant is 48[30], it is found in Fig.6.4 that the two-slot applicator has an impedance with highly mismatch. Its impedance rotates on a smith chart from an inductive

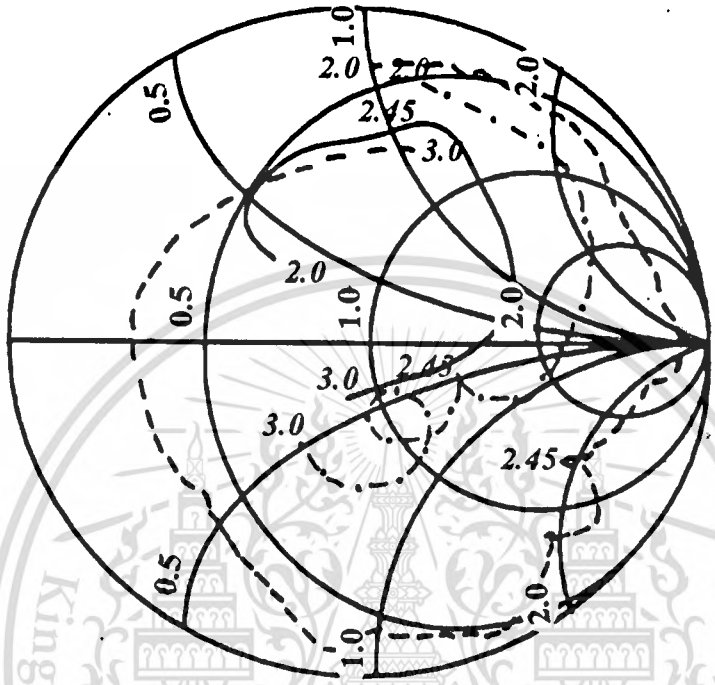

Fig.6.4 Input impedance of the applicators

- - - - - - two-slot applicator

——————— three-slot applicator

-·-·-·-·- four-slot applicator

impedance at 2.0 GHz to capacitive and becomes an inductive impedance at 3.0 GHz. For the three-slot applicator, the impedance changes from an inductive at 2.0 GHz and becomes capacitive at 3.0 GHz. At the operating frequency, its impedance is inductive with lower mismatch. The four-slot applicator behaves as an inductive impedance at the lower portion of the testing frequency and becomes a capacitive impedance at the higher frequency.The

impedance at the operating frequency is capacitive and is the closest one to 50 ohms.The VSWR of the two-slot, three-slot and four-slot applicators are 3.35, 2.16 and 1.13, respectively. Also their reflection coefficient are 0.54, 0.4 and 0.05, respectively. When these applicators are directly contact with a planar phantom, the VSWR are drastically increased due to the fact that there is a free space region between the applicator and a phantom surface. Consequently, in application with planar structure a water bolus must be designed so that its shape is the same as the free space area between the applicator and the heating material. This bolus will not only behave as a cooling system of the surface but also as a field matching device.

Table 6.1 Design Data and Experimental Performance of TM_{02} Mode Applicator with Different Number of Slots

number of slots	2	3	4
a(cm)	4.3	4.3	4.3
b(cm)	5.3	5.3	5.3
θ_c(°)	54.5	54.5	54.5
θ_0(°)	45	45	45
ϕ_{0i}(°)	0,180	0,120,240	0,90,180,270
slot length(cm)	9.25	6.0	4.5
penetration depth from the interface (cm)	1.9	3.0	2.9
EFS of the desired hotspot (cm^2)	5.1	7.7	13.8
net power for 235 W/kg (W)	111	98	93

6.4 Temperature-Time Relationship

In hyperthermia application it is desirable to elevate the tumor temperature up to a hyperthermic range (42°-45°C). It means that the temperature rise in the tumor is in the range of 5°-8°C higher than the normal temperature of a human body (37°C). In addition the rate of temperature rise should be kept around 1°C/minute so as not to injure the patient. An experiment was performed to get the information to design a hyperthermia system that satisfied such requirements. In the experiments, a planar human muscle phantom and a three-slot applicator with a 4 mm thick water bolus were prepared. The water temperature is 22°C with the flowrate of 0.5 litre/minute. In order to elevate the temperature at the depth of 2 cm up to 6°C with the rate of about 1°C/minute, a net power of 42W was applied to the applicator for first 8 minutes. Then, the power was reduced to 17W to retain the constant temperature. Temperature at three points i.e. at the surface, 1 cm and 2 cm depth along the central region of the applicator were measured using the fiber thermometers.

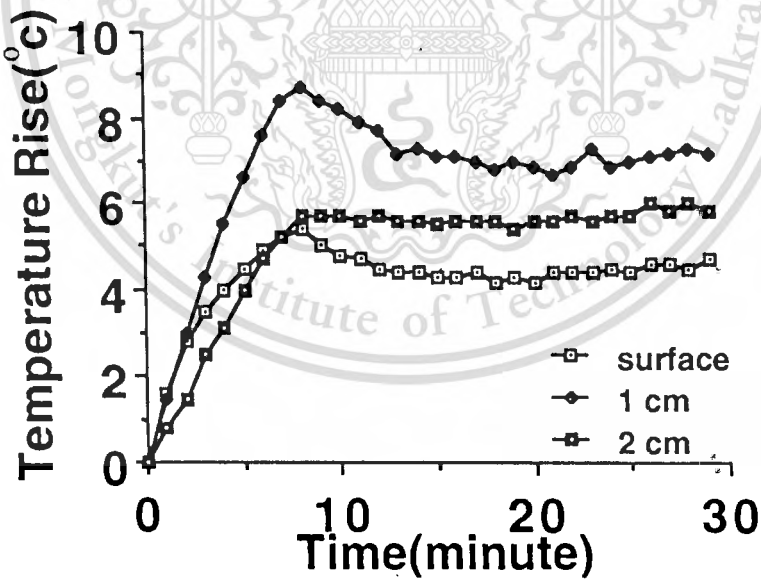

Fig.6.5 Temperature-Time relationship

From the experimental results, it is found that the rate of temperature rise ΔT are shown in Fig.6.5, temperature rise at the surface is 1.25°C/minute in the first 2 minutes, and then it falls down due to thermal diffusion in cooling water. It is expected that the surface temperature can be lowered if the water temperature is decreased. For the depth of 1cm, temperature rise is around 1.25°C/minute in the first 8 minutes. The maximum temperature rise at this depth is in excess of 9°C which is 1°C higher than the hyperthermic range. This problem can be solved by controlling bolus temperature and the power. It is seen that this three-slot applicator is useful for hyperthermia.

6.5 Heating Patterns

The muscle equivalent phantom is composed of 0.4 % NaCl, 0.02 % NaN_3 and 4 % Agar. The experiments were performed to illustrate the focusing effect in spherical phantom and to evaluate hotspot size in planar phantom. The two-slot applicator as mentioned in the previous section were employed to heat a spherical phantom with a radius of 4.3 cm.

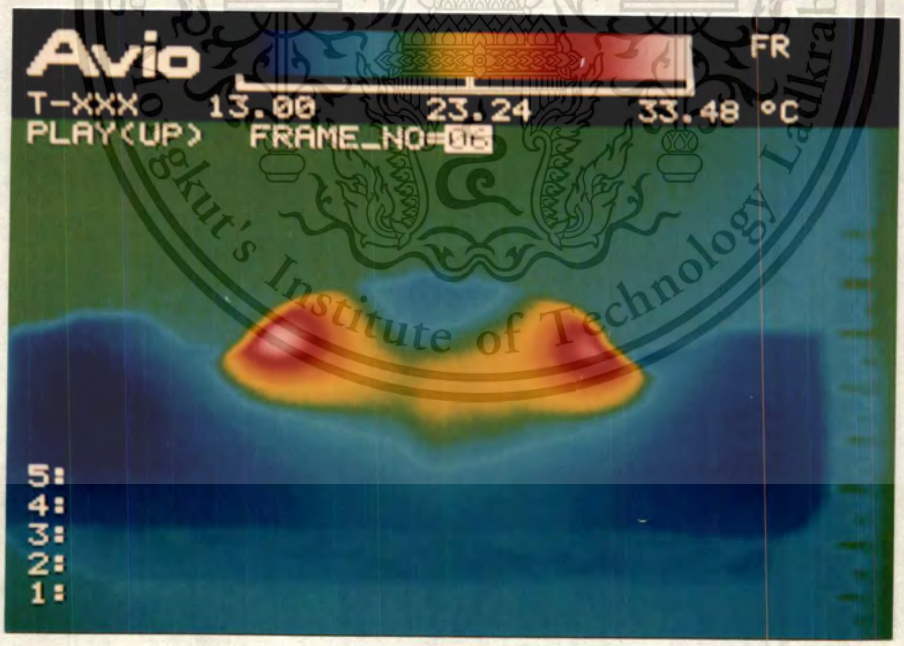

(a) without bolus

Fig.6.6 Heating patterns in spherical medium

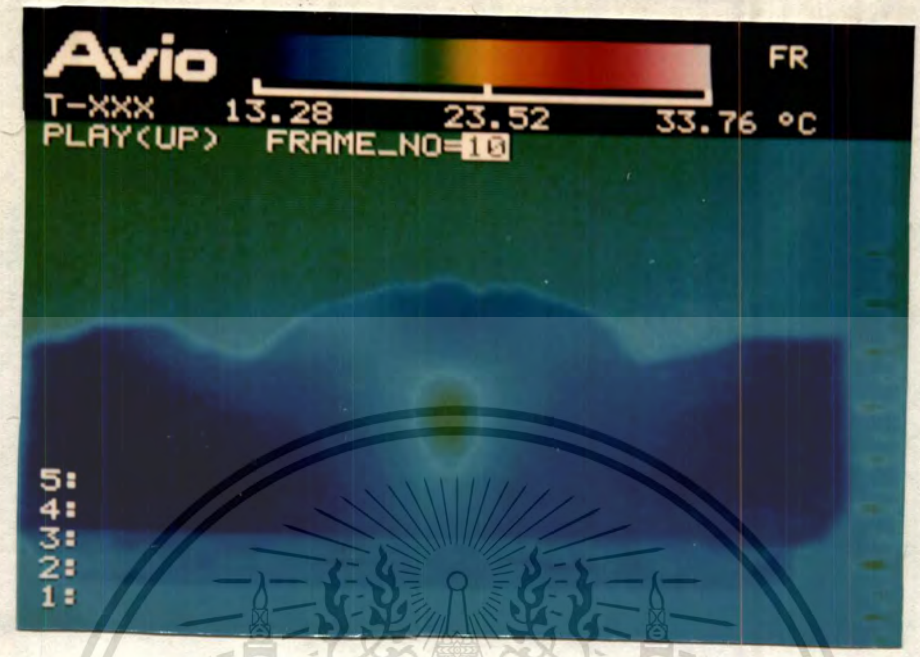

(b) with bolus

Fig.6.3 (cont'd)

Fig.6.6(a) shows a heating pattern on x-z plane after 85 W net power, (incident power-reflected power) was exposed . It is observed that there are two undesirable hotspots near the slot apertures and the field from each slot are combined at the central region of the spherical phantom. In application the desirable hotspot is only the central one, and then the other two hotspots closes to the slots should be eliminated. This can be achieved by using a cold water bolus (12-14 °C), of which the shape is concentric spherical plastic bag with 2 mm seperation with the water flow rate of 0.5 litre/minute. There remains only a desirable hotspot which EFS is 1.0 cm^2 and penetration depth is 2.5 cm at the central region of the spherical phantom as shown in Fig.6.6(b). This experimental result implies that when an appropriate cold water bolus is applied, this applicator can be used to perform local heating in the spherical part of a human body efficiently.

For a planar phantom experiment, Fig.6.7 shows the dimensions of the phantom and water bolus incorporated with the measuring planes.

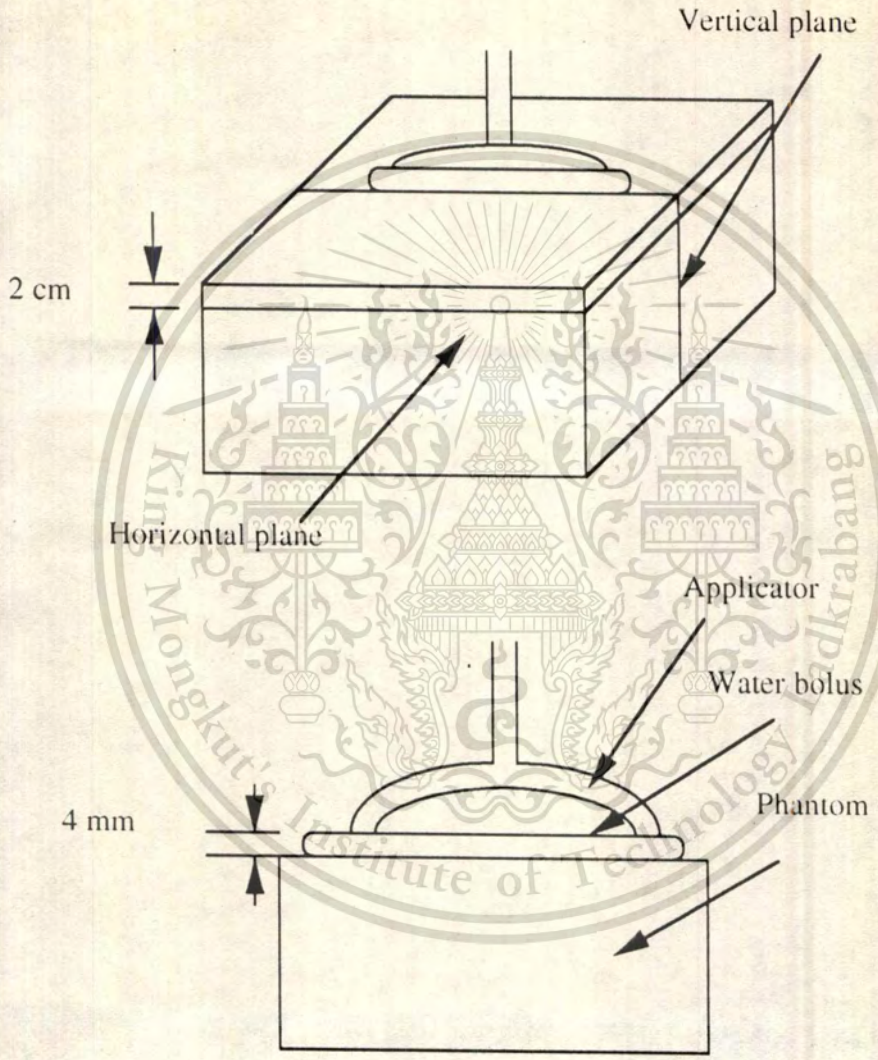

Fig.6.7 Dimension of the phantom and water bolus

Thermographs of a four-slot applicator with the net power of 119 W is shown in Fig.6.8.

(a) vertical-plane

(b) horizontal-plane

Fig.6.8 Thermograph of a four-slot applicator

Fig.6.8(a) shows the heating pattern on the vertical plane which implies that the penetration depth is about 3 cm. The heating pattern on the horizontal plane 2 cm deep from the surface is shown in Fig.6.8(b). On this plane from this figure, the EFS is about 13.8 cm^2 and it looks like a rectangle where the vertices are in the direction of each slot. It is evident that the size and shape of the hotspots can be varied by using different number of slot. The more the number of slots, the larger the size of the hotspot. This results from the reason that the slot lengths are decreased as the number of slots are increased. It is also observed that the maximum temperature rise is increased as the number of slots is increased. Moreover it is noted that the maximum heating depth is about 3 cm. It is deeper than a conventional open waveguide counterpart which the maximum depth is always limited to a skin depth about 1.7 cm [13].

It is recommended that applicators intended for therapy should be capable of producing SAR values of 235 W/kg in the muscle region [31]. From the experimental results of heating patterns mentioned above, we can calculate the net input power required for obtaining that value in the muscle region by measuring $(dT/dt)|_{t=0}$ from (3.4). The input powers are illustrated in Table 6.1. It is seen that the input power becomes lower by increasing a number of the slot.

6.6 Conclusion

This chapter presents some experimental results, performed at 2450 MHz, of the proposed applicator. It is found from radiation patterns that the focusing characteristics are achievable. The applicator with the higher number of slots possesses the lower VSWR. In order to design the microwave hyperthermia using this applicator, the power source should supply a power of 42 watts on the starting period to elevate the heating temperature to a hyperthermic range, then it is reduced to 17 watts to retain the constant temperature. From thermographic studies, we found that the heating volume can be varied by using different number of slots and the maximum heating depth is 3 cm.

Chapter 7

Discussions and Conclusions

As mentioned before, the main purpose of this thesis is to describe the research- study results about the spherical slot array applicator. So, this thesis is sub-divided into sub-sequence chapter as stated in introduction, chapter 1.

The derivation of the electromagnetic field expressions from a slot on a perfectly conducting sphere are introduced in the most beginning chapter, chapter 2, to reveal a lot of interesting and fundamental concepts and strategy to be developed in the subsequence chapters.

An investigation about the electric field from an array of slots on part of conducting sphere are manipulated in chapter 3 to ensure, at least theoretically, that the focusing capability of the electromagnetic field from the slot array on partial conducting sphere still appears as in the case of complete conducting sphere. In this chapter, a Specific Absorption Rate (SAR) which describes the performance of applicator is also studied and some numerical results are carried out. One of the most interesting results is the effective field size of the applicator can be taken care by adjusting the number of slots.

In chapter 4 a concentric conducting spherical cavity has been proposed as a means to excite a spherical slot array. Since the proposed configuration, which is excited by an electric field probe, is suited for a transverse magnetic wave. Therefore, a TM to r spherical wave function has been introduced to investigate the field inside the cavity. Then proper boundary conditions are applied and the design of the cavity has been obtained. Comparisons of Q-factor of different modes have been illustrated. Experiments have been performed on a TM_{02} cavity and it is found in good agreement with the theoretical predictions.

In chapter 5 the concept of a focus array has been introduced. Then the particular configuration of a concentric conducting spherical cavity-backed slot array applicator has been described. Theoretical performance of two-slot applicators excited by different cavity modes have been

illustrated. It is found that the applicator made of a TM_{02} cavity is suitable for focusing electric field deepen into the heated material. However it is not ready in clinical application because of the additional undesirable hotspots, so it is necessary to eliminate them. One of advisable means is to employ a water bolus. The particular water bolus that is suitable for the applicator has also been discussed in this chapter.

In chapter 6 the performance of the proposed applicator have been investigated experimentally. Radiation patterns of a one-slot, two-slot and three-slot applicators have been measured in a simulated human muscle phantom. It is satisfactory that the field focusing capability appears as in theoretically prediction. Observation on input impedance of a two-slot, three-slot and four-slot applicators reveals that the applicator with the higher number of slots, implies the shorter slot, possesses the lower VSWR. The resultant temperature-time relationship shows that, in designing a microwave hyperthermia system using this kind of applicator, the power source should supply high power on the starting period to elevate the heating temperature to a hyperthermic range, then it is reduced to the moderate level to retain the constant temperature. Eventually, thermographic studies confirm that the water bolus can eliminate the undesirable hotspots efficiently. The heating volume, that means the tumor size, can be treated by using the applicator with different number of slots.

The research in this thesis is restricted to a homogeneous human muscle. However, the human body is actually inhomogeneous. Therefore, investigation on the application of this applicator in a inhomogeneous medium by assuming multiple layers of concentric spherical medium is of interest. In addition, for a larger spherical model such as a human head, studying of frequency scaling to suit the spherical size is challenging. Theoretical investigation of input impedance of this kind of applicator has not been performed. Moreover, an application of an applicator using a TM_{01} cavity mode should be suitable and a steerable focusing array by inserting some particular material in the cavity is interesting and opened for further study.

References

[1] J.C.Lin," Foreward," IEEE Trans. Microwave Theory Tech., vol.MTT-34, No.5, pp.481-483, May 1986.

[2] I.J.Bahl, S.S.Stuchly and M.A. Stuchly," A New Microstrip Radiator for Medical Applications," IEEE Trans. Microwave Theory Tech., vol.MTT-28, No.12, pp.1461-1468, Dec.1980.

[3] M.A.Stuchly, S.S.Stuchly and G.Kantor," Diathermy Applicators with Circular Aperture and Corrugated Flange," IEEE Trans. Microwave Theory Tech., vol. MTT-28, No.3, pp.267-271, Mar. 1980.

[4] I.J.Bahl, S.S.Stuchly and M.A.Stuchly," New Microstrip Slot Radiator For Medical Applications," Electronics Letters, vol.16, No.19, pp.731-732, Sep.1980.

[5] Y.X.Wang," Slot-Line Coupler for Medical Applications," Electronics Letter, vol.20, No.22, pp.939-940, Oct.1984.

[6] R.H. Johnson," New Type of Compact Electromagnetic Applicator for Hyperthermia in the Treatment of Cancer," Electronics Letter, vol.22, No.11, pp.591-593, May 1986.

[7] R. Leedee, M. Chive and M. Plancot," Microstrip Microslot Antennas for Biomedical Applications: Frequency Analysis of Different Parameters of This Type of Applicator," Electronics Letters, vol.21, No.7, pp.304-305, Mar. 1986.

[8] N.K. Vzunoglu, E.A. Angelikas and P.A. Cosmidis," A 432-MHz Local Hyperthermia System Using an Indirectly Cool,Water-Loaded Waveguide Applicator," IEEE Trans. Microwave Theory Tech., vol.MTT-35, No.2, pp.106-111, Feb. 1987.

[9] J. Loane, H.Ling, B.F.Wang and S.W. Lee," Experimental Investigation of a Retro-Focusing Microwave Hyperthermia Applicator: Conjugate-Field Matching Scheme," IEEE Trans. Microwave Theory Tech., vol.MTT-34, No.5, pp.490-494, May 1986.

[10] J.W. Hand, J.L. Cheetham and A.J. Hind," Absorbed Power Distributions from Coherent Microwave Arrays for Localized Hyperthermia," IEEE Trans. Microwave Theory Tech., vol.MTT-34, No.5, pp.484-489, May 1986.

[11] W.Gee, S.W.Lee, N.K.Bong, C.A.Cain, R.Mittra and R.L.Magin," Focused Array Hyperthermia Applicator: Theory and Experiment," IEEE Trans. Biomedical Engineering, vol. BME-31, No.1, pp.38-46, Jan. 1984.

[12] J.R. James, C.M. Hall and G.Andrasic," Angled Dual Compact Hyperthermia Applicators," IEE Proceedings, vol.134, Pt.H, No.3, pp.315-320, June 1987.

[13] Y.Nikawa, H. Watanabe, M. Kikuchi and S. Mori," A Direct-Contact Microwave Lens Applicator with a Microcomputer-Controlled Heating System for Local Hyperthermia," IEEE Trans.Microwave Theory and Tech., vol.MTT-34, No.5, pp.626-630, May 1986.

[14] Y. Nikawa, T. Katsumata, M.Kikuchi and S.Mori," An Electric Field Converging Applicator with Heating Pattern Controller for Microwave Hyperthermia," IEEE Trans.Microwave Theory Tech., vol.MTT-34, No.5, pp.631-635, May 1986.

[15] Y. Nikawa and F.Okada," Dielectric-Loaded Lens Applicator for Microwave Hyperthermia," IEEE Trans. Microwave Theory Tech., vol.39, No.7,pp.1173-1178, July 1991.

[16] A.W. Guy, C.K.Chou and K.H. Luk," 915-MHz Phased Array System for Treating Tumors in Cylindrical Structures," IEEE Trans. Microwave Theory Tech., vol.MTT-34, No.5, pp.502-507, May 1986.

[17] M. Krairiksh, T. Wakabayashi and W. Kiranon," Characteristics of Microwave Applicator Using Slots On a Sphere," Medical and Biological Engineering and Computing, vol.29, Supplement Part1, pp. 425, 1991.

[18] M. Krairiksh, T. Wakabayashi and W. Kiranon," Microwave Applicator Using Two Slots on Sphere," Proceedings of the Fourth Asia-Pacific Microwave Conference, Adelaide, pp.225-228, 1992.

[19] M.Krairiksh, T.Wakabayashi and W.Kiranon," A Spherical Slot Array Applicator for Medical Applications," to be published in IEEE Trans. Microwave Theory Tech.

[20] S.G.Zhu and K.M.Chen, Correction to "Interaction of the Near-Zone Field of a Slot on a Conducting Spherical Model of Man," IEEE Trans. Microwave Theory Tech., vol.MTT-33, No.4, pp.350-351, April 1985.

[21] M. Krairiksh, T. Wakabayashi and W. Kiranon," Analysis of Interior Electromagnetic Fields from a Slot on a Perfectly Conducting Sphere," Proceedings of the Third Asia-Pacific Microwave Conference, Tokyo, pp.1183-1186, 1990.

[22] J.A.Stratton,"Electromagnetic Theory," McGraw-Hill, 1941.

[23] S.G.Zhu, K.M.Chen and H.R.Chuang," Interaction of the Near-Zone Fields of a Slot on a Conducting Sphere with a Dielectric Sphere," Technical Report No.1 NSF Grant ECS-8001772-01 National Science Foundation, Washington, June 1983.

[24] A.W.Guy," Analysis of Electromagnetic Fields Induced in Biological Tissues by Thermographic Studies on Equivalent Phantom Models," IEEE Trans. Microwave Theory Tech., vol. MTT-19, pp.205-214, Feb. 1971.

[25] M.V. Prior, M.L.D. Loumori, G.R. Forse and J.W. Hand,"Current Sheet Applicator Arrays for Superficial Hyperthermia: Incoherent versus Coherent Operation," Medical and Biological Engineering and Computing, vol.29, Supplement Part 1, pp. 425, 1991.

[26] C.A.Balanis,"Advanced Engineering Electromagnetics," John Wiley and Sons, 1989.

[27] S.A.Schelkunoff," Electromagnetic Waves," D.Van Norstrand, 1943.

[28] R.F.Harrington," Time-Harmonic Electromagnetic Fields," McGraw-Hill, 1961.

[29] J.P.Holman," Heat Transfer," McGraw-Hill, 1981.

[30] G. Gajda, M.A. Stuchly and S.S. Stuchly," Mapping of the Near-Field Pattern in Simulated Biological Tissues," Electronics Letters, vol.15, No.4, pp.120-121, Feb. 1979.

[31] R.H. Johnson, J.R. James, J.W. Hand, J.W. Hopewell, P.R.C. Dunlop and R.J. Dickinson, "New Low-Profile Applicators for Local Heating of Tissues," IEEE Trans. Biomedical Engineering, vol. BME-31, No.1, Jan. 1984.

Related Publications

1. M.Krairiksh, T.Wakabayashi and W.Kiranon, "Analysis of Interior Electromagnetic Fields from a Slot on a Perfectly Conducting Sphere," The 3rd Asia-Pacific Microwave Conference Proceedings, Tokyo, pp.1183-1186, 1990.

2. M.Krairiksh and K.Panichpathompong,"Interior Fields of Slot on Sphere," The 29th Kasetsart University Annual Conference, Bangkok, pp.687-699, 1991.

3. M.Krairiksh, T.Wakabayashi and W.Kiranon," Characteristics of Microwave Applicator Using Slots on Sphere," Digest of The World Congress on Medical Physics and Biomedical Engineering" ,Kyoto, pp.425, 1991.

4. M Krairiksh, S.Kosulvit, K.Wayuphak and P.Noiram," Concentric Conducting Spherical Cavity," Proceedings of The 14th Conference on Electrical Engineering, Songkhla, pp.4-22 to 4-25, 1991.

5. M.Krairiksh, T.Wakabayashi and W.Kiranon," Microwave Applicator Using Two Slots on Sphere," Proceedings of The Fourth Asia-Pacific Microwave Conference, Adelaide, pp.225-228, 1992.

6. M.Krairiksh and W.Kiranon," A Concentric Conducting Spherical Cavity-Backed Slot Array, "Proceedings of The 15th Conference on Electrical Engineering, Bangkok, pp.2-39 to 2-44, 1992.

7. M.Krairiksh, W.Kiranon and T.Wakabayashi," A Microwave Hyperthermia System Using Slot Array Applicator," Abstract of 2nd Far Eastern Conference on Medical and Biological Engineering, Beijing, pp.184, 1993.

8. M.Krairiksh, T.Wakabayashi and W.Kiranon," A Spherical Slot Array Applicator for Medical Applications," to be published in IEEE Transactions on Microwave Theory and Techniques.